



Mid-crustal deformation of the Annapurna-Dhaulagiri Himalaya, central Nepal: An atypical example of channel flow during the Himalayan orogeny

A.J. Parsons^{1,*}, R.J. Phillips¹, G.E. Lloyd¹, R.D. Law², M.P. Searle³, and R.D. Walshaw¹

¹School of Earth and Environment, University of Leeds, Leeds, West Yorkshire LS2 9JT, UK

²Department of Geosciences, Virginia Polytechnic Institute and State University, Blacksburg, Virginia 24061-0002, USA

³Department of Earth Sciences, University of Oxford, Oxford OX1 3AN, UK

ABSTRACT

The channel-flow model for the Greater Himalayan Sequence (GHS) of the Himalayan orogen involves a partially molten, rheologically weak, mid-crustal layer “flowing” southward relative to the upper and lower crust during late Oligocene–Miocene. Flow was driven by topographic overburden, underthrusting, and focused erosion. We present new structural and thermobarometric analyses from the GHS in the Annapurna-Dhaulagiri Himalaya, central Nepal; these data suggest that during exhumation, the GHS cooled, strengthened, and transformed from a weak “active channel” to a strong “channel plug” at greater depths than elsewhere in the Himalaya. After strengthening, continued convergence resulted in localized top-southwest (top-SW) shortening on the South Tibetan detachment system (STDS). The GHS in the Annapurna-Dhaulagiri Himalaya displays several geological features that distinguish it from other Himalayan regions. These include reduced volumes of leucogranite and migmatite, no evidence for partial melting within the sillimanite stability field, reduced structural thickness, and late-stage top-southwest shortening in the STDS. New and previously published structural and thermobarometric constraints suggest that the channel-flow model can be applied to mid-Eocene–early Miocene mid-crustal evolution of the GHS in the Annapurna-Dhaulagiri Himalaya. However, pressure-temperature-time (PTt) constraints indicate that following peak conditions, the GHS in this region did not undergo rapid isothermal exhumation and widespread sillimanite-grade decompression melting, as commonly recorded elsewhere in the Himalaya. Instead, lower-than-typical structural thickness and melt volumes suggest that the upper part of the GHS (Upper Greater Himalayan Sequence [UGHS]—the proposed channel) had a greater viscosity than in other Himalayan regions. We suggest that viscosity-limited, subdued channel flow prevented exhumation on an isothermal trajectory and forced the UGHS to exhume slowly. These findings are distinct from other regions in

the Himalaya. As such, we describe the mid-crustal evolution of the GHS in the Annapurna-Dhaulagiri Himalaya as an *atypical* example of channel flow during the Himalayan orogeny.

1. INTRODUCTION

The kinematic and metamorphic evolution of the metamorphic core of the Himalayan orogen (Fig. 1), referred to as the Greater Himalayan Sequence (GHS), is the central focus of all models of Himalayan orogenesis (e.g., Grujic et al., 1996; Beaumont et al., 2001; Bollinger et al., 2006; Robinson et al., 2006; Searle et al., 2006; Kohn, 2008; Mukherjee, 2013b; He et al., 2014; Cottle et al., 2015; Frassi, 2015; Montomoli et al., 2015). The channel-flow model for the Himalayan orogen proposes that the GHS represents a rheologically weak, partially molten, mid-crustal channel that flowed laterally southward, between the upper and lower bounding rigid crust. Flow was driven by lithostatic loading by the Tibetan plateau, underthrusting of the Indian lower crust, and focused erosion at the orogenic front (Fig. 2) (Beaumont et al., 2001; Godin et al., 2006a; Harris, 2007). Extrusion and exhumation of the channel were facilitated by coeval shearing along the top-to-the-south (top-S) Main Central thrust zone (MCTZ) and top-to-the-north (top-N) South Tibetan detachment system (STDS), which bound the GHS below and above, respectively (see reviews by Godin et al., 2006a; Grujic, 2006).

Many of the geological and geophysical constraints on which the channel-flow model is based (e.g., pressure-temperature [PT] conditions and crustal thicknesses) are derived from the Everest, Sikkim, and Bhutan regions (e.g., Grujic et al., 1996, 2002) of the central-eastern Himalaya (Fig. 1A). In these regions, the channel-flow model provides a robust explanation for the kinematic, dynamic, and temporal evolution of the GHS (e.g., Nelson et al., 1996; Beaumont et al., 2001; Searle and Szulc, 2005; Unsworth et al., 2005; Searle et al., 2006; Streule et al., 2010). However, the lithologic, structural, and metamorphic framework of the GHS varies along the ~2500 km length of the orogen. It thus remains unclear the extent to which the channel-flow model can be applied along the whole orogen (Godin et al., 2006a; Harris, 2007).

*Current address: Geological Survey of Canada, 1500–605 Robinson Street, Vancouver, B.C. V5B 5J3, Canada

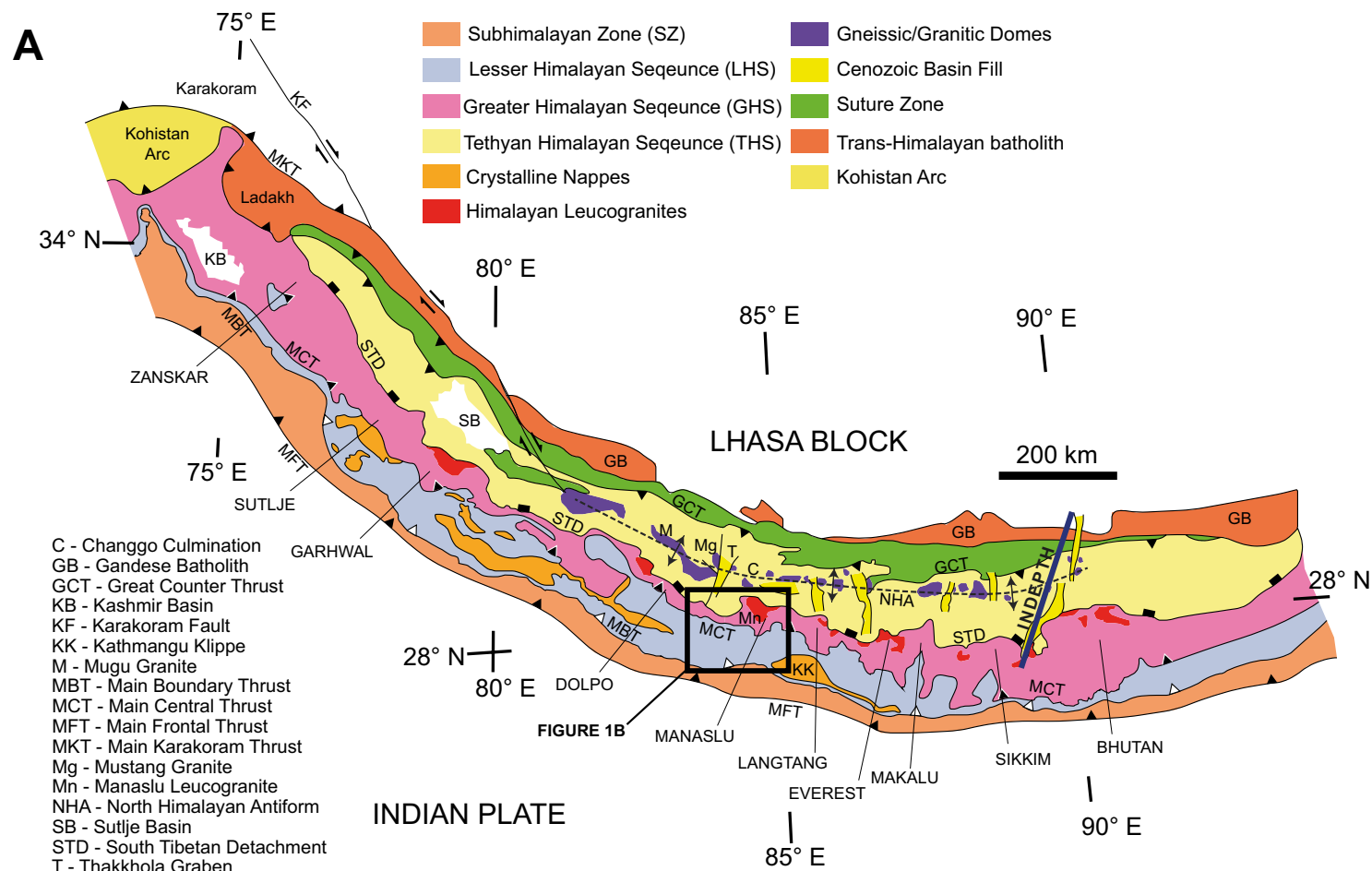


Figure 1 (on this and following page). (A) Simplified geological sketch map of the Himalayan orogen (after Goscombe et al., 2006; Searle et al., 2008; and Law et al., 2013). Blue line indicates approximate location of INDEPTH profile (Nelson et al., 1996).

In this study, the applicability of the channel-flow model to the GHS in the Annapurna-Dhaulagiri Himalaya in central Nepal (Fig. 1) is tested through a synthesis of new structural and thermobarometric analyses of the metamorphic rocks, combined with previously published geochronometric and thermobarometric constraints. Field observations from the Modi Khola and Kali Gandaki valleys (Fig. 1B) reveal geological features of the GHS that are atypical when compared to other Himalayan regions along strike. These include reduced volumes of leucogranite and migmatite, an absence of evidence for partial melting within the sillimanite stability field, reduced structural thickness, and late-stage top-SW shortening on the STDS following cessation of top-NE

extensional shearing. The presence of such features has significant implications for the rheology of the GHS and raises the question of whether or not the GHS in this region was weak enough for mid-crustal flow.

1.2. Channel Flow during the Himalayan Orogeny

Channel flow describes the laminar flow of a viscous fluid between upper and lower rigid plates (Turcotte and Schubert, 2002). Flow can be driven by horizontal pressure gradients (*Poiseuille flow*) and/or motion of the channel walls (*Couette flow*). When a pressure gradient and channel-wall motion are

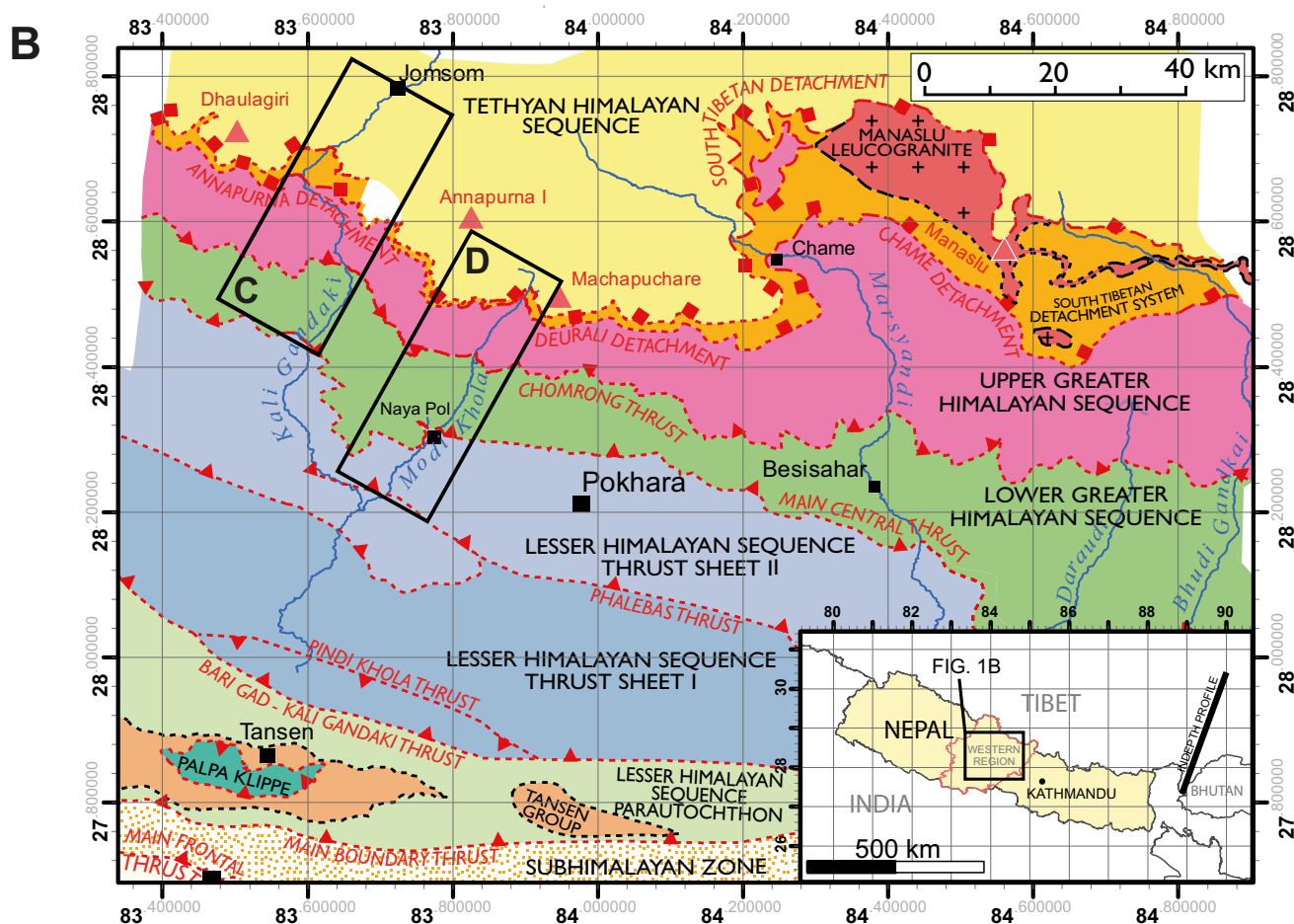


Figure 1 (continued). (B) Simplified tectonostratigraphic map of Western Region, Nepal. Major tectonic units and bounding faults and shear zones are labeled. Black boxes show extent of (C) Kali Gandaki and (D) Modi Khola transects (Plates 1 and 2). Inset map shows field area location in relation to the rest of Nepal. Red outline defines Western Region. After Parsons et al. (2016).

applied in opposite directions, a *hybrid flow* may form (Grujic, 2006) in which a portion of the channel flows in the opposite direction to the moving channel wall (the “return flow” of Mancktelow, 1995).

In applying the channel-flow model to the Himalaya, it is proposed that the GHS is an exhumed portion of a mid-crustal channel (Beaumont et al., 2001; Godin et al., 2006a; Harris, 2007). After initial collision between India and Eurasia, crustal thickening and heating followed by widespread partial melting at mid-crustal levels resulted in the development of a weak, low-viscosity channel located between rigid upper and lower crust (Beaumont et al., 2001; Godin et al., 2006a). Upon weakening below a threshold viscosity, southward return flow of the mid-crustal channel initiated. This flow was driven by a horizontal gradient in lithostatic pressure produced by the relative topographic elevations

and crustal thicknesses of the Tibetan plateau and Indian continent, and from shear stresses due to the northward underthrusting of the lower Indian continental crust (Beaumont et al., 2001, 2004; Grujic, 2006). Focused erosion aided exhumation of the channel to the orogenic front (Beaumont et al., 2001). Relatively low viscosities were maintained during exhumation due to continued partial melting along an isothermal exhumation path (Harris and Massey, 1994; Streule et al., 2010; Jamieson et al., 2011; Searle, 2013).

Application of the channel-flow model to the Himalayan orogen places a crucial dependence on widespread partial melting of the mid-crust for the required reduction in viscosity (Beaumont et al., 2001, 2004; Grujic, 2006; Jamieson et al., 2011). Finite element thermomechanical models of channel flow simulate this strength drop by changing the rheology of elements within

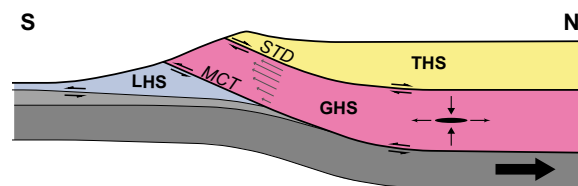


Figure 2. Channel-flow model for the Himalayan orogen. Yellow—Tethyan Himalayan Sequence (THS); pink—Greater Himalayan Sequence (GHS); blue—Lesser Himalayan Sequence (LHS); light gray—Indian Upper crust; dark gray—Indian Lower Crust; MCT—Main Central thrust; STD—South Tibetan detachment. Thick black arrow shows northward motion of Indian Lower Crust. Gray arrows in GHS represent velocity relative to the down-going slab. Black arrows and ellipse show vertical shortening + horizontal stretching of GHS. Based on Godin et al. (2006a).

the modeled crust from a stress- and temperature-dependent power-law rheology based on experimentally derived flow laws (e.g., Blackhill Quartzite; Gleason and Tullis, 1995) to a “melt weakened” linear viscous rheology with a viscosity of 10^{19} Pa s once the temperature exceeds 700 °C (Beaumont et al., 2001, 2004; see also experimental verification of assumed viscosities by Rutter et al., 2011). This imposed reduction in viscosity simulates the order of magnitude drop in rheological strength expected to occur during widespread partial melting of the crust (Rosenberg and Handy, 2005; Rosenberg et al., 2007). Experimental deformation of rocks shows that an increase in melt fraction from 0.00 to 0.07 (i.e., 7%) is accompanied by a ~90% reduction in strength, referred to as the melt-connectivity transition (MCT, Rosenberg and Handy, 2005). An intermediate strength drop is also recorded between a melt fraction of 0.20 and 0.50, which corresponds to the solid-liquid transition (SLT; Rosenberg and Handy, 2005). Consequently, determining the extent and duration of partial melting within the GHS is crucial for validating the channel-flow model for the Himalayan orogen.

The extent to which channel-flow models are representative of the whole of the Himalaya has also been questioned (Godin et al., 2006a; Harris, 2007). The original thermomechanical channel-flow model (Beaumont et al., 2001) was based on seismic reflection and magneto-telluric data from the INDEPTH transect (Nelson et al., 1996), conducted across the southern part of the Tibetan plateau to the north and east of Sikkim, India (Fig. 1). The channel was modeled as a homogeneous layer; whereas the GHS comprises a lower portion of greenschist-facies quartzites, marbles, and metapelitic rocks and an upper portion of amphibolite-facies pelitic, psammitic, and calc-silicate paragneisses and schists, orthogneiss, and migmatites. While lithologies in individual tectonostratigraphic units within the GHS are remarkably constant along the length of the Himalaya, the relative proportions of these lithologies do vary (Le Fort, 1975; Upreti, 1999; Yin, 2006) and are likely to have produced orogen-parallel variations in viscosity during mid-crustal evolution. Additionally, thermomechanical channel-flow models suggest that a minimum channel thickness of 10–20 km is required for crustal flow to be an effective form of ex-

trusion, although this thickness may change slightly for different model resolutions (Beaumont et al., 2004; Jamieson et al., 2004, 2006). The thickness of the GHS varies along the length of the orogen, and it remains unclear whether sections with a structural thickness of <10 km are too thin to have pervasively deformed by channel flow (Beaumont et al., 2004; Godin et al., 2006a). In order to test applicability of the model to the whole orogen, it is crucial, therefore, to assess the validity of the channel-flow model in regions of the Himalaya that differ from those where the model is best suited.

1.3. The Annapurna-Dhaulagiri Himalaya

The Himalayan orogeny initiated at ca. 50 Ma during final closure of Neotethys (Searle, 1986; Green et al., 2008; Najman et al., 2010) (Fig. 1A). Since this time, the Himalayan belt has been under a continuous state of convergence, resulting in uplift and erosion of the world's highest mountain peaks (e.g., Searle et al., 2011; Avouac, 2015; Searle, 2015). In central Nepal, the Himalaya can be divided into four tectonic units separated by orogen-parallel faults and shear zones (Fig. 1B). From SW to NE, these units are the Subhimalayan Zone (SZ), the Lesser Himalayan Sequence (LHS), the Greater Himalayan Sequence (GHS), and the Tethyan Himalayan Sequence (THS) (Le Fort, 1975; see extensive reviews by Dhital, 2015).

The central Himalaya in Western Region, Nepal, is dominated by the peaks of Annapurna I (8091 m) and Dhaulagiri (8167 m) (Fig. 1B). Access through the region is gained along the NE-SW-trending Modi Khola and Kali Gandaki valleys and the foothills between. The geology of the region was first described by Le Fort (1975), was subsequently mapped in detail (Colchen et al., 1981; Hodges et al., 1996; Godin, 2003; Martin et al., 2010; Searle, 2010; Parsons et al., 2016), and is the subject of numerous detailed structural, thermobarometric, and geochronometric studies (Bouchez and Pêcher, 1981; Arita, 1983; Le Fort et al., 1986; Pêcher, 1989; Brown and Nazarchuk, 1993; Nazarchuk, 1993; Kaneko, 1995; Hodges et al., 1996; Vannay and Hodges, 1996; Godin et al., 1999a, 1999b, 2001; Godin, 2003; Bollinger et al., 2004; Martin et al., 2005; Paudel and Arita, 2006; Kellett and Godin, 2009; Larson and Godin, 2009; Martin et al., 2010; Corrie and Kohn, 2011; Kohn and Corrie, 2011; Carosi et al., 2015; Iaccarino et al., 2015; Larson and Cottle, 2015; Martin et al., 2015).

2. TECTONOSTRATIGRAPHY AND STRUCTURAL FRAMEWORK

In the Annapurna-Dhaulagiri Himalaya (Plates 1 and 2), the GHS is bound below by the Main Central Thrust (MCT) and above by the South Tibetan detachment (STD) and is divided here into the Lower GHS (LGHS), Upper GHS (UGHS), and South Tibetan detachment system (STDS). The LGHS and UGHS are separated by the Chomrong thrust (CT), while the UGHS and STDS are separated by the Annapurna detachment (AD) in the Kali Gandaki valley and the Deurali detachment (DD) in the Modi Khola valley. Internally, the UGHS is deformed by the Kalopani shear zone (KSZ) in the Kali Gandaki valley and the Modi Khola shear zone (MKSZ) in the Modi Khola valley (Hodges et al., 1996;

989

KALI GANDAKI TRANSECT

Vertical scale = Horizontal scale

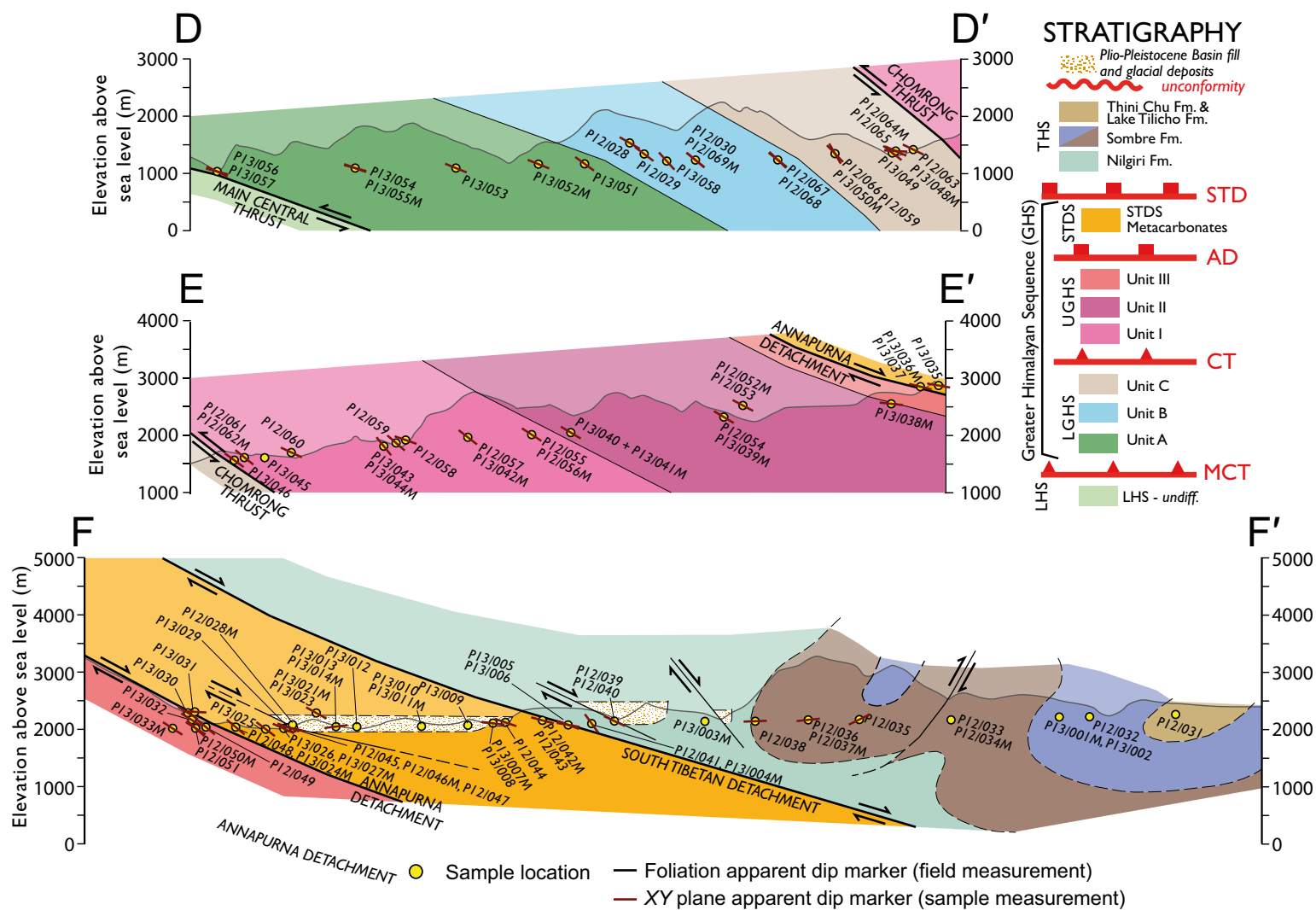


Figure 3. Cross sections through the Kali Gandaki valley. Relative structural positions of samples are shown. Structural foliation and sample-derived kinematic XY plane apparent orientations are displayed with dip ticks. See Plate 1 for section locations. AD—Annapurna detachment; CT—Chomrong thrust; GHS—Greater Himalayan Sequence; LGHS—Lower Greater Himalayan Sequence; LHS—Lesser Himalayan Sequence; MCT—Main Central thrust; STD—South Tibetan detachment; STDS—South Tibetan detachment system; THS—Tethyan Himalayan Sequence.

MODI KHOLA TRANSECT

Vertical scale = Horizontal scale

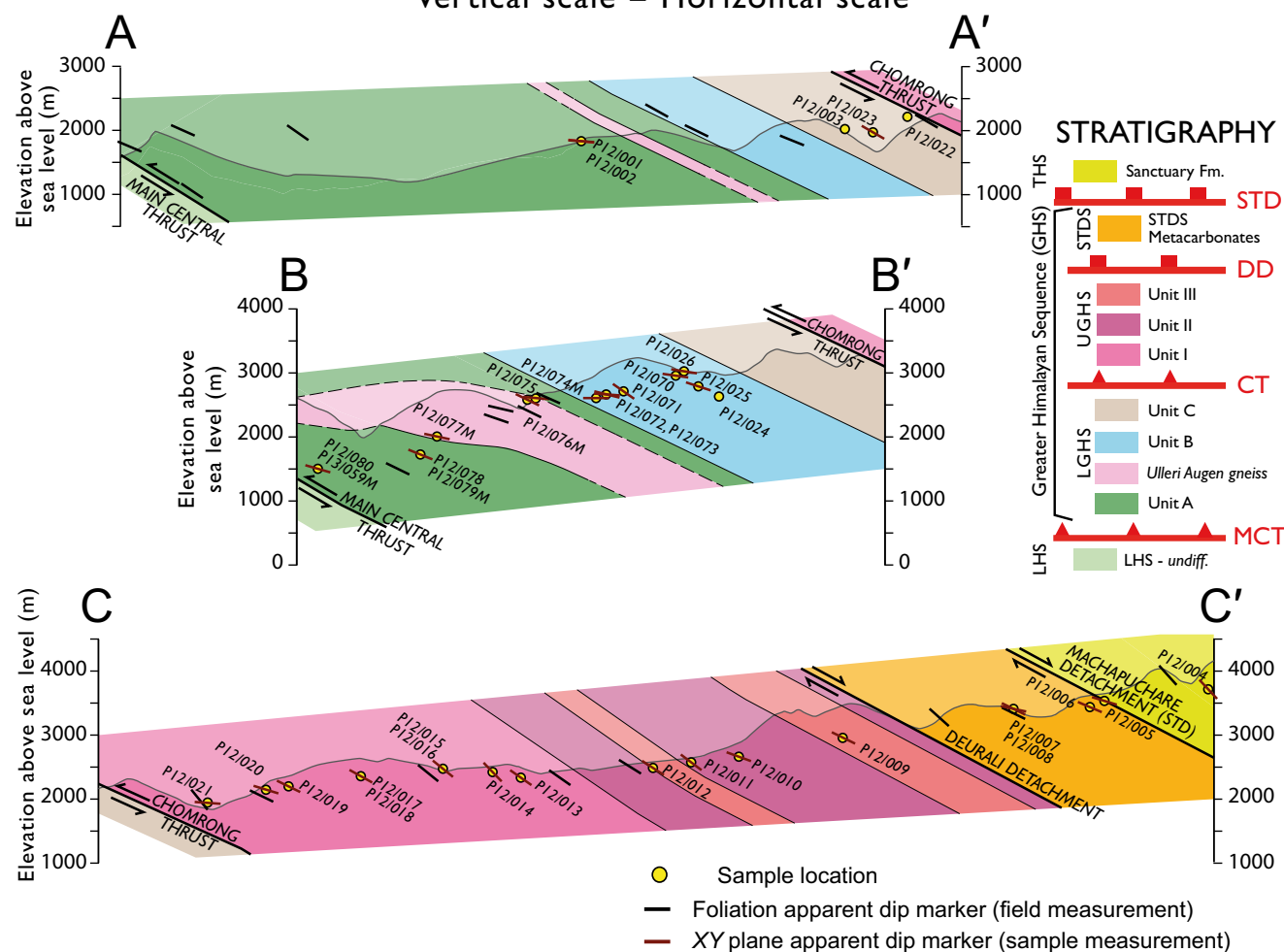


Figure 4. Cross sections through the Modi Khola valley. Relative structural positions of samples are shown. Structural foliation and sample-derived kinematic XY plane apparent orientations are displayed with dip ticks. See Plate 2 for section locations. Acronyms are same as for Figure 3; DD—Deurali detachment.

Regional foliation (S3) dips approximately NE, with mineral lineation trends ranging between NW and E (Fig. 5). A general parallelism observed between the orientation of the regional S3 foliation, C-planes of localized S-C fabrics (*sensu* Berthé et al., 1979), and the major bounding shear zones suggests that S3 is a shear-related transpositional fabric, as observed in the LGHS and STDS (see below). Top-SW S3 shear indicators are observed throughout the UGHS (Figs. 6A, 6C, and 6D). The upper portion of the UGHS is deformed

by the top-SW Kalopani shear zone (KSZ; Vannay and Hodges, 1996) and Modi Khola shear zone (MKSZ; Hodges et al., 1996) in the Kali Gandaki (Plate 1) and Modi Khola valleys, respectively. Subordinate S4 deformation structures associated with deformation on the KSZ and MKSZ are observed locally across the UGHS, deforming the regional S3 foliation (Plate 1 and Fig. 6D). Late-stage, N-S-striking normal faults and fracture sets (S5) are observed in the Kali Gandaki transect (Fig. 5).

TABLE 1A. SUMMARY OF DEFORMATION FABRIC GENERATIONS IN THE ANNAPURNA-DHAULAGIRI HIMALAYA

| Fabric generation | LGHS | UGHS | STDS | THS (from Godin, 2003) |
|-------------------|---|--|--|---|
| S0 (bedding) | n/a | n/a | n/a | Deformed by km-scale F2 folds |
| S1 | Microscopic fabric preserved in pelites. Deformed by S2 + S3. | n/a | n/a | Subparallel to bedding; deformed by km-scale F2 folds |
| F1 | n/a | n/a | n/a | S1 parallel isoclinal folding |
| S2 | Microscopic fabric preserved in pelites. Crenulation cleavage deforms S1 foliation. | n/a | n/a | Crenulation cleavage axial planar to km-scale F2 folds, deforms S1 and S0 |
| F2 | n/a | n/a | n/a | Overtured to upright km-scale folds with NW-SE–striking hinge planes |
| S3 | NE-dipping, regional transpositional fabric, parallel to structural and lithological boundaries, related to top-SW shearing | NE-dipping, regional transpositional fabric, parallel to structural and lithological boundaries, related to top-SW and top-NE shearing | ENE- to E-dipping, regional transpositional fabric, parallel to structural and lithological boundaries, related to top-SW shearing | STDS parallel foliation. Present at base of THS, deforms S1 and S2 |
| L3 | NE-plunging regional mineral stretching lineation | NE- to E-plunging regional mineral stretching lineation | E-plunging regional mineral stretching lineation | n/a |
| F3 | Localized folding related to top-SW shearing | Localized folding related to top-SW shearing. Subparallel to S3 | Localized folding related to top-ENE shearing | Regional shear-related fold transposes S1 and S2 into parallelism with S3 |
| S4 | E-W–striking, subvertical crenulation cleavage in pelitic rocks deforms S3. | Subparallel to S3. Syn- to postmetamorphic top-SW shear fabric. | Subparallel to S3. Syn- to postmetamorphic top-SW shear fabric. | Subparallel to S3, always steeper, with associated thrust faults |
| F4 | n/a | n/a | Localized folding related to top-SW shearing deforms S3 foliation and leucogranite bodies. | Kink folds deform S1, S2, S3 |
| S5 | N-S–striking normal faults and associated subvertical joint set | N-S–striking normal faults and associated subvertical joint set | N-S–striking normal faults and associated subvertical joint set | N-S–striking, subvertical cleavage. Normal faults and associated penetrative cleavage |

Note: Based on classifications of Godin (2003). Abbreviations: LGHS—Lower Greater Himalayan Sequence; UGHS—Upper Greater Himalayan Sequence; STDS—South Tibetan detachment system; THS—Tethyan Himalayan Sequence; n/a—no data.

TABLE 1B. MEAN FABRIC ORIENTATIONS IN THE GREATER HIMALAYAN SEQUENCE

| Fabric generation | Transect | MCT | LGHS | UGHS | Unit I | Unit II | Unit III | STDS |
|-------------------|--------------|--|-----------|-----------|-----------|-----------|-----------|-----------|
| S3 | Modi Khola | S planes—058/57 NW; C planes—075/39 NW | 119/25 NE | 116/42 NE | n/a | n/a | n/a | 112/36 NE |
| S3 | Kali Gandaki | S planes—156/63 NE; C planes—147/24 NE | 128/36 NE | 118/38 NE | 112/48 NE | 109/35 NE | 145/36 NE | 157/29 E |
| L3 | Modi Khola | 31/030 | 19/028 | 29/097 | n/a | n/a | n/a | n/a |
| L3 | Kali Gandaki | n/a | 41/028 | n/a | 41/022 | 29/000 | 29/078 | 16/087 |
| S4 | Kali Gandaki | n/a | n/a | n/a | n/a | n/a | n/a | 151/41 E |
| F4 | Kali Gandaki | n/a | n/a | n/a | n/a | n/a | n/a | 129/28 NE |
| S5 | Kali Gandaki | n/a | 178/70 W | 192/83 W | n/a | n/a | n/a | 195/76 E |

Note: Abbreviations: MCT—Main Central thrust; LGHS—Lower Greater Himalayan Sequence; STDS—South Tibetan detachment system; n/a—no data.

2.2.2. UGHS Metamorphic and Geochronometric Constraints (Previous Work)

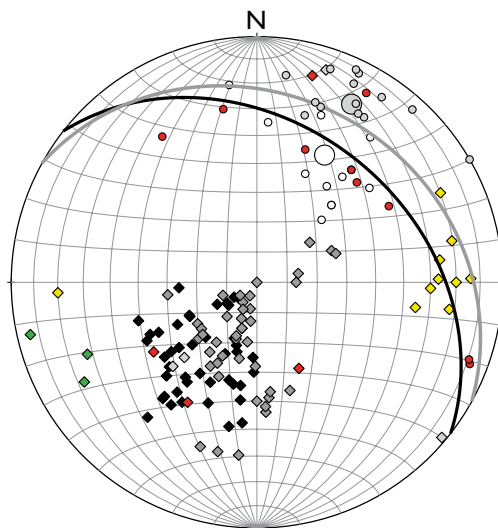
The UGHS in the Annapurna-Dhaulagiri Himalaya equilibrated within the kyanite stability field (Carosi et al., 2015). No evidence has been found for partial melting within the sillimanite stability field (Nazarchuk, 1993; Hodges et al., 1996; Larson and Godin, 2009). In the Modi Khola transect, peak meta-

morphic temperatures and pressures of 750–825 °C and 11–14 kbar are recorded (garnet-biotite cation exchange [GARB] thermometry—Kaneko, 1995; GARB and garnet-ilmenite cation exchange thermometry, garnet-plagioclase-quartz-muscovite (GPMQ), and garnet-plagioclase-aluminosilicate-quartz (GASP)—phase equilibria barometry—Martin et al., 2010; GARB and Zr-in-titanite thermometry, GPMQ, GASP, and garnet-plagioclase-biotite-quartz (GPBQ)—phase equilibria barometry—Corrie and Kohn, 2011).

GHS STRUCTURAL DATA

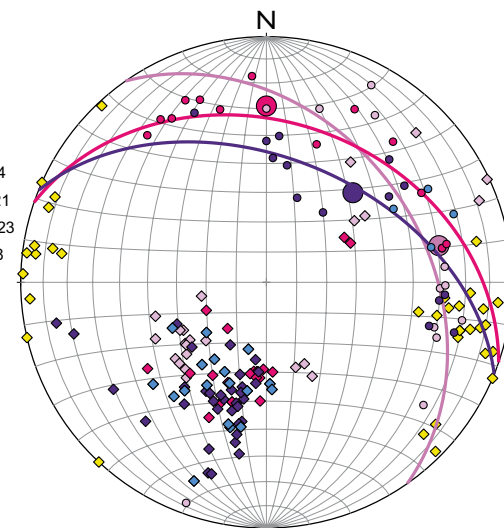
A LGHS

- S3 mean foliation (Kali Gandaki)
- S3 mean foliation (Modi Khola)
- ◆ S3 pole to foliation (Kali Gandaki) n = 44
- ◆ S3 pole to foliation (Modi Khola) n = 41
- ◆ S5 pole to foliation (Kali Gandaki) n = 10
- ◆ Poles to cren. cleavage (Kali Gandaki) n = 4
- ◆ Poles to fault planes (Kali Gandaki) n = 3
- L3 mean lineation (Kali Gandaki)
- L3 mean lineation (Modi Khola)
- L3 lineation (Kali Gandaki) n = 10
- L3 lineation (Modi Khola) n = 16
- Fold axes (Kali Gandaki) n = 10
- ◆ Poles to axial planes (Kali Gandaki) n = 4



B UGHS

- S3 mean foliation - Unit I (Kali Gandaki)
- S3 mean foliation - Unit II (Kali Gandaki)
- S3 mean foliation - Unit III (Kali Gandaki)
- ◆ S3 poles to foliation - Unit I (Kali Gandaki) n = 34
- ◆ S3 poles to foliation - Unit II (Kali Gandaki) n = 21
- ◆ S3 poles to foliation - Unit III (Kali Gandaki) n = 23
- ◆ S3 poles to foliation - Undiff. (Modi Khola) n = 18
- ◆ S5 poles to foliation (Kali Gandaki) n = 34
- L3 mean lineation - Unit I (Kali Gandaki)
- L3 mean lineation - Unit II (Kali Gandaki)
- L3 mean lineation - Unit III (Kali Gandaki)
- L3 lineation - Unit I (Kali Gandaki) n = 14
- L3 lineation - Unit II (Kali Gandaki) n = 13
- L3 lineation - Unit III (Kali Gandaki) n = 13
- L3 lineation - Undiff. (Modi Khola) n = 4



C STDS

- S3 mean foliation (Kali Gandaki)
- S4 mean foliation (Kali Gandaki)
- ◆ S3 poles to foliation (Kali Gandaki) n = 44
- ◆ S3 poles to foliation (Modi Khola) n = 2
- ◆ S4 poles to foliation (Kali Gandaki) n = 7
- ◆ S5 poles to foliation (Kali Gandaki) n = 3
- L3 mean lineation (Kali Gandaki)
- L3 lineation (Kali Gandaki) n = 19
- F4 fold axes (Kali Gandaki) n = 3
- F4 poles to axial planes (Kali Gandaki) n = 3
- ◆ Poles to fault planes (Kali Gandaki) n = 4

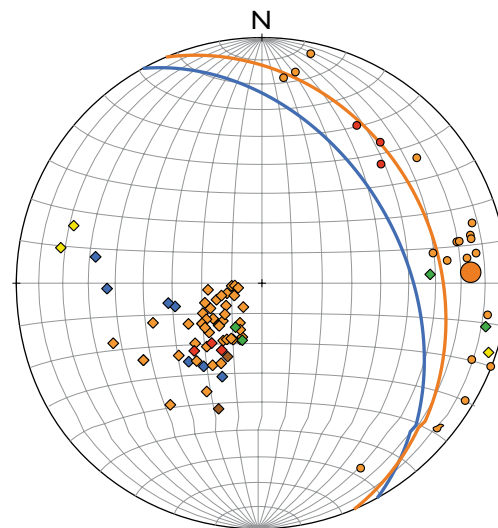


Figure 5. Structural data from the Greater Himalayan Sequence (GHS). All data plotted on lower hemisphere equal area projections; geographic north indicated. (A) Lower Greater Himalayan Sequence (LGHS); (B) Upper Greater Himalayan Sequence (UGHS); (C) South Tibetan detachment system (STDS). UGHS and STDS mean plane and lineation orientations derived from Kali Gandaki transect only. See Table 1B for summary of mean orientations. See Supplemental File 1 (footnote 1) for full structural data set.

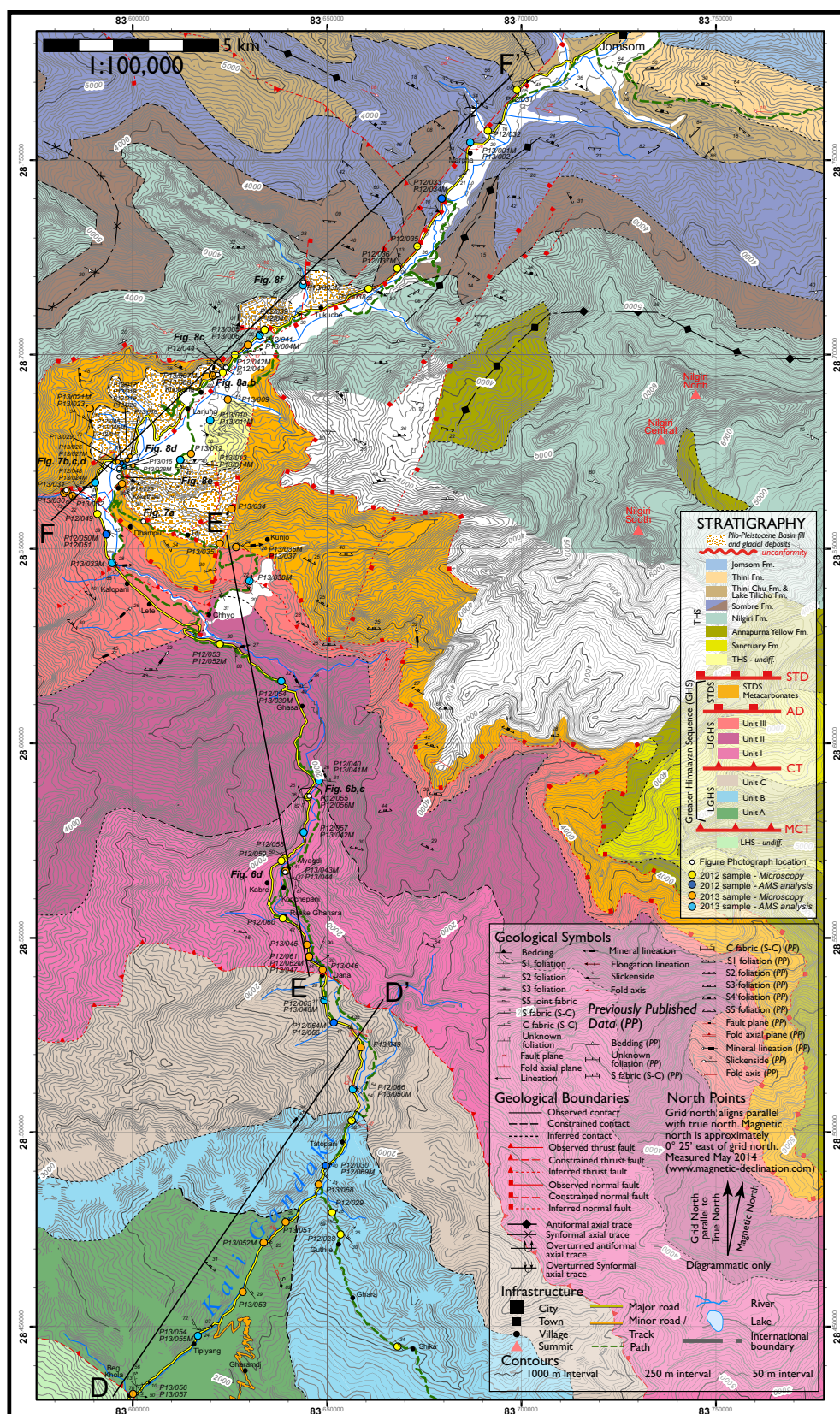


Plate 1. 1:100,000 geological map of the Kali Gandaki valley. Locations of field photographs (Figs. 6–8), cross sections (Fig. 3), and photomicrographs (Figs. 6 and 9) are given, along with locations of all samples collected during fieldwork. Abbreviations are as follows: AD—Annapurna detachment; AMS—Anisotropy of magnetic susceptibility; CT—Chomrong thrust; LGHS—Lower Greater Himalayan Sequence; LHS—Lesser Himalayan Sequence; MCT—Main Central Thrust; STD—South Tibetan detachment; STDs—South Tibetan detachment system; THS—Tethyan Himalayan Sequence. To view Plate 1 at full size, please visit <http://dx.doi.org/10.1130/GES01246.S4> or the full-text article on www.gsapubs.org.

To view Plate 1 at full size, please visit
<http://dx.doi.org/10.1130/GES01246.S4>
 or the full-text article on www.gsapubs.org.

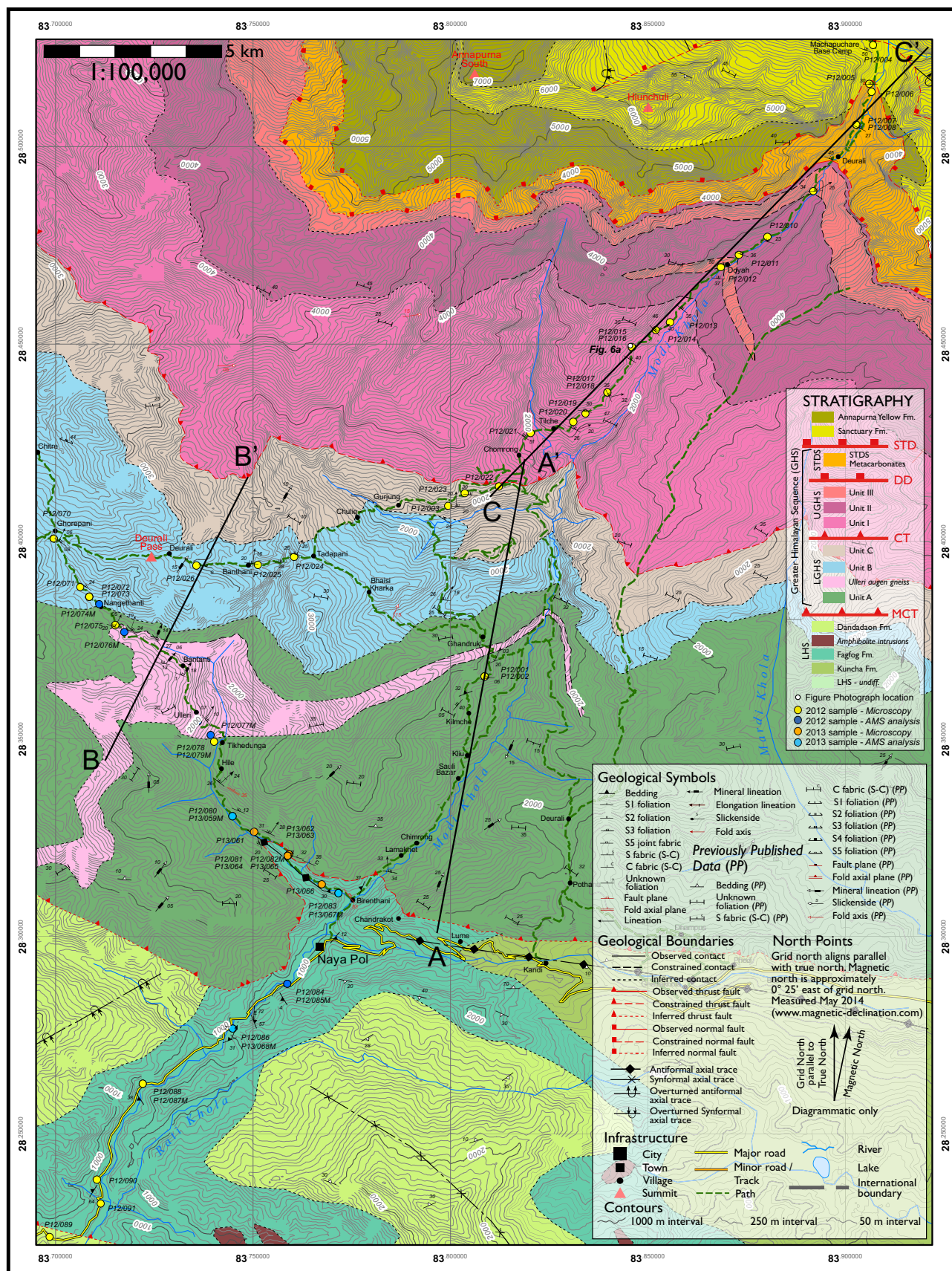


Plate 2. 1:100,000 geological map of the Modi Khola valley. Locations of field photographs (Fig. 6) and cross sections (Fig. 4) are given, along with locations of all samples collected during fieldwork. To view Plate 2 at full size, please visit <http://dx.doi.org/10.1130/GES01246.S5> or the full-text article on www.gsapubs.org.

To view Plate 2 at full size, please visit
<http://dx.doi.org/10.1130/GES01246.S5>
or the full-text article on www.gsapubs.org.

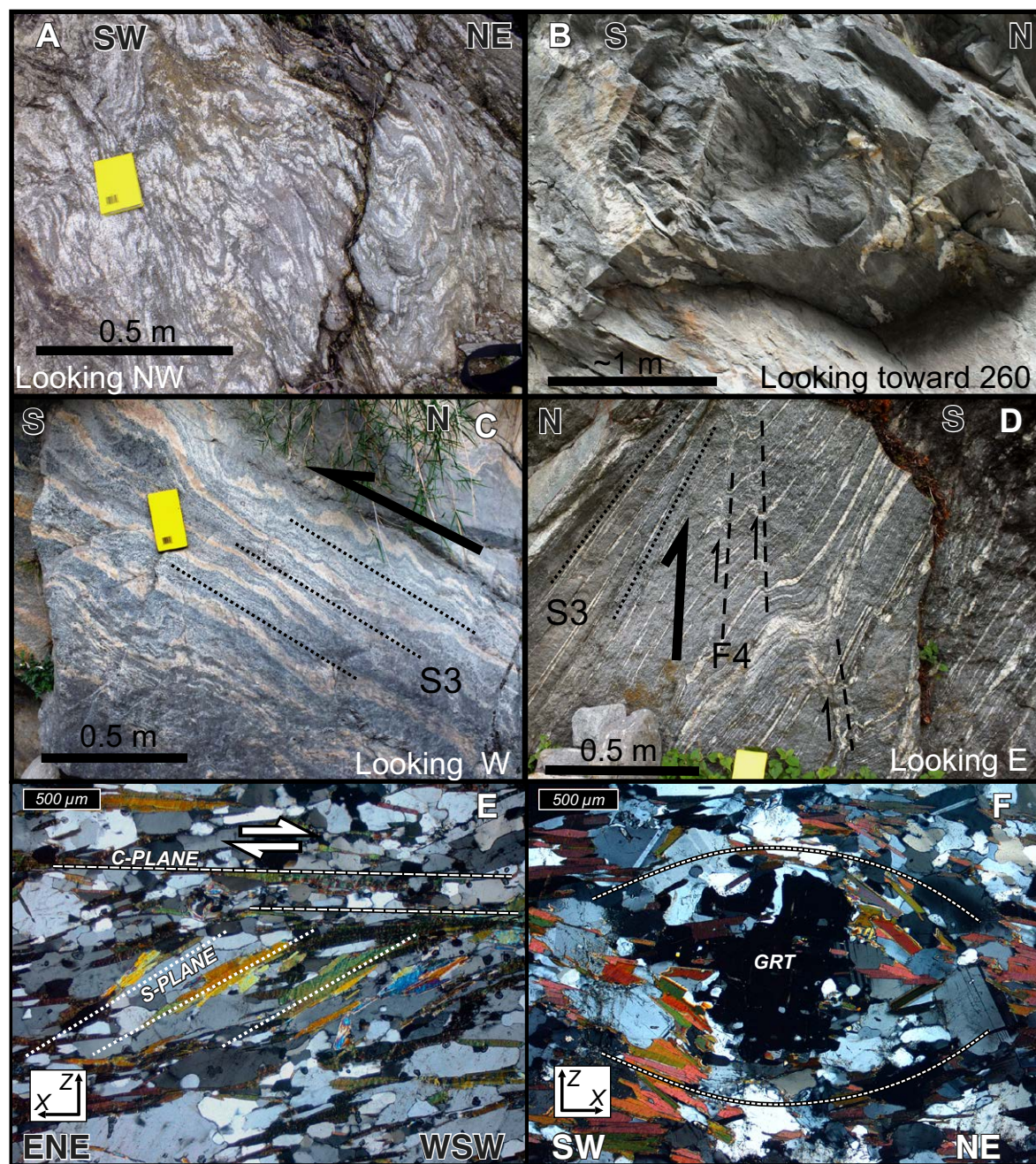


Figure 6. Leucosome structures and shear-sense indicators in the Upper Greater Himalayan Sequence (UGHS). See Plates 1 and 2 for photo locations and Figure 3 for relative structural positions of sample photomicrographs. (A) Folded leucosomes in Unit I migmatite from the Modi Khola transect. (B) Amorphous leucosome bodies in Unit I, Kali Gandaki transect. (C) Banded leucosomes in Unit I migmatites in the Kali Gandaki transect. Leucosomes record top-S shearing along S3 foliation-parallel shear planes. Deformation features suggest that deformation occurred during partial melting, prior to crystallization of leucosomes. (D) Banded leucosomes in Unit I migmatites in the Kali Gandaki transect. The S3 leucosome fabric is deformed by S4 thrust-tip folds. (E) Sample P13/046–Unit I, Kali Gandaki. Top-WSW S-C fabric from hanging wall of the Chomrong thrust. (F) Sample P12/059–Unit I, Kali Gandaki. Microstructures around garnet porphyroblast (GRT) with no discernible shear sense. All micrographs viewed in XZ plane of kinematic reference frame.

A range of temperatures and pressures is recorded from the UGHS in the Kali Gandaki transect. Iaccarino et al. (2015) recorded peak temperatures and pressures of 710–720 °C and 10–11 kbar from garnet-muscovite-biotite-ilmenite multiphase equilibria thermobarometry and Zr-in-rutile thermometry. Le Fort et al. (1986) recorded temperatures and pressures of ~650–700 °C and 5–10 kbar from GARB-GASP thermobarometry. Vannay and Hodges (1996) recorded temperatures and pressures of ~500–750 °C and 6–12 kbar from GARB and garnet-hornblende cation exchange thermometry and GASP, garnet-rutile-aluminosilicate-ilmenite-quartz, garnet-plagioclase-muscovite-biotite, and garnet-amphibole-plagioclase-quartz phase equilibria barometry. It is likely that the use of different thermobarometer calibrations and analytical methods to select appropriate element compositions has contributed to some of the differences in pressure and temperature estimates between these studies (e.g., Hodges and McKenna, 1987; Kohn and Spear, 2000; Kohn, 2014). Quartz *c*-axis fabric opening angle thermometry (Kruhl, 1998) from Unit I in the Kali Gandaki valley records a deformation temperature of 670 ± 50 °C (Larson and Godin, 2009).

U-Pb zircon and monazite geochronology and titanite thermochronology in the Annapurna-Dhaulagiri Himalaya indicate prograde metamorphism of the UGHS at temperatures exceeding 700 °C, initiated at 48–43 Ma (Carosi et al., 2015; Iaccarino et al., 2015; Larson and Cottle, 2015). Peak metamorphic temperatures were attained between 35 and 30 Ma in Unit III and 28–20 Ma in Unit I and Unit II (Corrie and Kohn, 2011; Kohn and Corrie, 2011; Iaccarino et al., 2015). In Unit I in the Kali Gandaki valley, retrogression from peak conditions began as early as 28 Ma and reached 650–670 °C and 7–8 kbar between 25 and 18 Ma (Iaccarino et al., 2015). This equates to a vertical exhumation from ~30–33 km to ~21–24 km at a time-averaged rate of 0.6–4.3 mm yr⁻¹. In the Modi Khola valley, Corrie and Kohn (2011) recorded retrogression of Unit I between 17 and 22 Ma. During metamorphism, partial melting initiated as early as 41 Ma and continued to as late as 18.5 Ma (Nazarchuk, 1993; Hodges et al., 1996; Godin et al., 2001; Corrie and Kohn, 2011; Kohn and Corrie, 2011; Carosi et al., 2015; Larson and Cottle, 2015; Iaccarino et al., 2015).

Crystallization ages of undeformed leucogranite dikes suggest that motion on the CT occurred before 22–18.5 Ma (Nazarchuk, 1993; Hodges et al., 1996). Uniform ⁴⁰Ar/³⁹Ar muscovite cooling ages from across the UGHS suggest that the sequence was extruded and exhumed to the topographic surface as a coherent single block at ca. 16–12 Ma (Vannay and Hodges, 1996; Godin et al., 2001; Martin et al., 2015).

2.3. South Tibetan Detachment System (STDS)

The STDS has a structural thickness of ~1700–2200 m and forms the uppermost part of the GHS, consisting of metacarbonates, marble, and subordinate calc-silicate gneiss. Marbles and metacarbonates within the STDS are dominated by calcite and contain variable proportions of quartz, plagioclase, and mica ± K-feldspar ± dolomite. Calc-silicate gneiss at the base of the STDS is composed of clinopyroxene, amphibole, clinozoisite, plagioclase, K-feldspar,

quartz, biotite, and calcite ± rutile ± titanite. Leucogranite sills and dikes are found in the lower to middle portions of the STDS. At the base of the STDS, the top-down-E Annapurna detachment (Plate 1, AD—Kali Gandaki valley, Brown and Nazarchuk, 1993) and the top-down-NE Deurali detachment (Plate 2, DD—Modi Khola valley, Hodges et al., 1996) form foliation-parallel, normal-sense mylonitic shear zones with deformed, foliation-parallel leucogranite sills (Fig. 7). At the top of the STDS, the STD forms a more discrete top-E to top-NE brittle-ductile normal-sense detachment between the GHS and THS (Plates 1 and 2; Burg et al., 1984).

The S3 foliation dips to the ENE and NE in the Kali Gandaki and Modi Khola valleys, respectively (Fig. 5). The L3 stretching lineation plunges E and NE in the Kali Gandaki and Modi Khola valleys, respectively (Fig. 5). The S3-parallel transposed calcite veins are common across the STDS. In the Kali Gandaki valley, S3 foliation is locally deformed by S4 foliation (Plate 1 and Fig. 5C) and folds with S3-associated normal (top-E—F3) and S4-associated reverse (top-SW—F4) senses of vergence (Plate 1; Figs. 7 and 8) are observed. Leucogranite intrusions in the STDS in the Kali Gandaki valley are also deformed by F4 folding (Fig. 8). In addition, deformation microstructures from the STDS, including rotated porphyroblasts and grain-shape-preferred orientations, record both top-E (S3) and top-SW shearing (S4) (Fig. 9). The youngest deformation in the STDS is defined by a set of N-S-striking, subvertical normal faults and fractures (S5).

U-Pb geochronology of deformed and undeformed leucogranites suggests that the DD was active at ca. 22.5 Ma (Hodges et al., 1996) and that motion on the AD had ceased by ca. 22 Ma (Godin et al., 2001). In the Modi Khola valley, the STD was active after 18.5 Ma but may have initiated before this time (Hodges et al., 1996).

2.4. Tethyan Himalayan Sequence (THS) and Mid-Miocene to Recent Sedimentation

The THS is bound by the STD (Plates 1 and 2) to the south and the Indus-Yarlung suture zone (IYSZ) to the north (Searle, 2010). The IYSZ is exposed in southern Tibet, north of the study area. In the Annapurna-Dhaulagiri Himalaya, the THS comprises weakly metamorphosed (chlorite-grade or lower) Cambro-Ordovician to Cretaceous limestones, dolostones, and marls belonging to the Annapurna, Sanctuary, Nilgiri, Sombre and Thini Chu, and Lake Tilicho formations (Plates 1 and 2). The full stratigraphic framework of the THS is described in detail by Gradstein et al. (1992), Garzanti (1999), and Godin (2003).

The structure of the THS in the Kali Gandaki valley has been extensively studied by Godin (2003) and is summarized in Table 1. Within the upper Kali Gandaki valley, the Thakkhola graben has deformed the THS since mid-Miocene times during E-W extension (Plate 1 and Fig. 3) and is responsible for the subvertical, N-S-striking S5 foliation recorded in the THS and GHS (Hurtado et al., 2001; Garzanti et al., 2003; Godin, 2003). Basin fill within the Thakkhola graben is mid-Miocene to Plio-Pleistocene in age (Garzanti et al., 2003; Adhikari and Wagerich, 2011; Baltz, 2012).

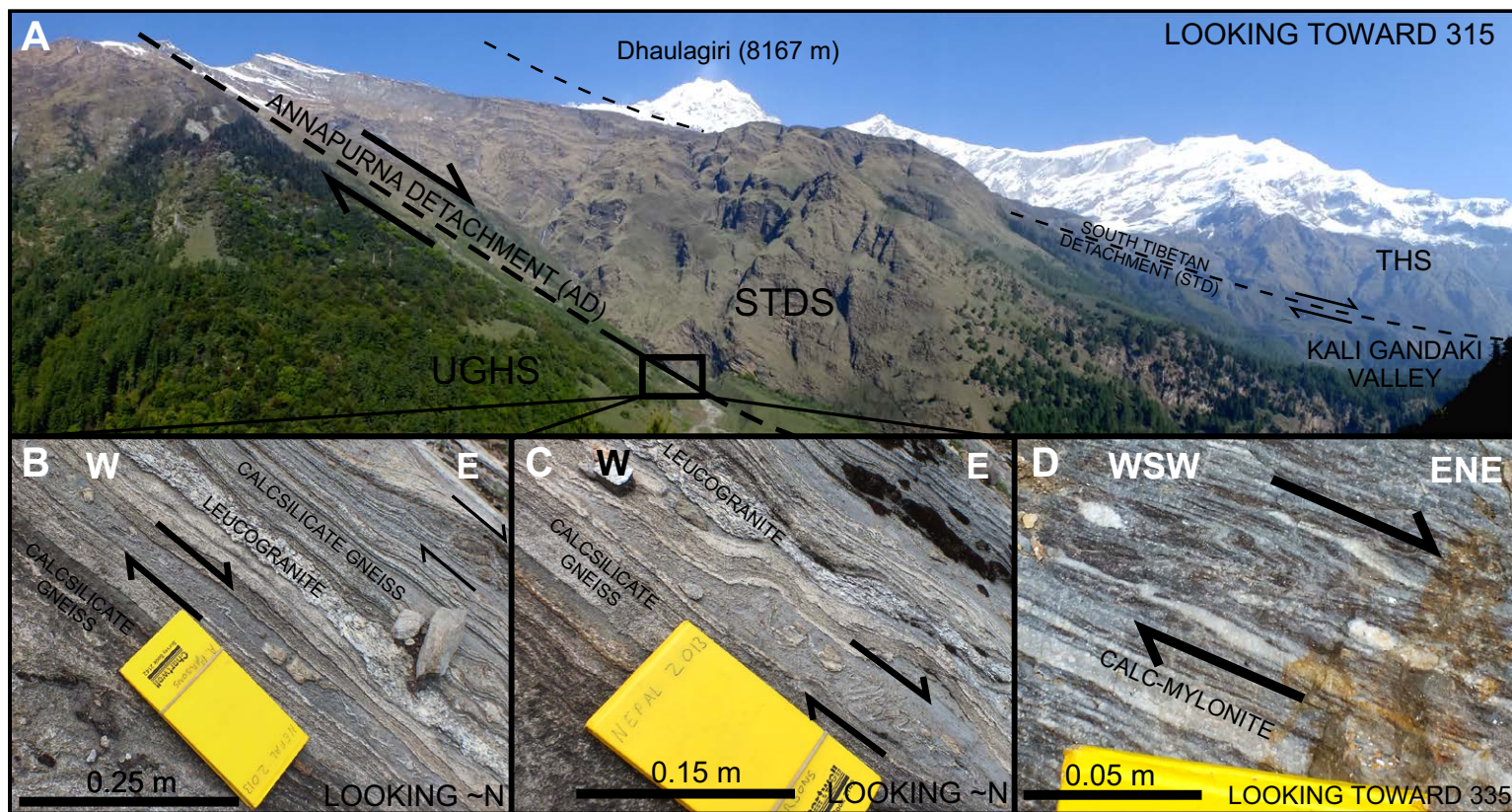


Figure 7. Annapurna detachment (AD) exposed on the Kali Gandaki transect. (A) Panoramic photograph of the AD, which is accessible at the mouth of the gorge highlighted by the small black box, where (B) and (C) are located. (B–C) Sheared and boudinaged calc-silicate gneiss and leucogranite from the AD, recording top-E normal-sense motion (S3). (D) Top-ENE normal-sense shearing (S3) recorded by a calc-mylonite from the AD, observed at a different location to (C). See Plate 1 for locations of photographs.

3. NEW THERMOBAROMETRIC CONSTRAINTS FOR THE GHS IN THE KALI GANDAKI VALLEY

New estimates of peak metamorphic temperatures and pressures for the UGHS in the Kali Gandaki valley have been determined via GARB and Zr-titanite thermometry and GASP barometry. All analyses were conducted using wavelength dispersive X-ray spectroscopy with a JEOL 8230 electron microprobe at the University of Leeds using *Probe for EPMA* (Probe Software, Inc.). A description of methods used during data acquisition and the analytical conditions for both analyses are provided in Supplemental File 2². The microprobe analysis data sets are included in Supplemental File 3³.

Three samples were selected for thermobarometry from Unit I of the UGHS in the Kali Gandaki transect (P12/055, P12/058, and P12/060; see Plate 1 for sample

locations). All samples contain garnet, biotite, plagioclase, kyanite, and quartz. Sample P12/060 also contains muscovite. Peak temperature and pressure estimates are based on major-element compositions of garnet, biotite, and plagioclase, calculated simultaneously using the “Thermobarometry With Estimation of EQUilibrium state” method (TWEEQU; Berman, 1991) with the winTWQ v2.32 software (Berman, 2007). This multi-equilibrium approach uses a single internally consistent thermodynamic database (Berman and Aranovich, 1996) to find the point at which multiple phase reactions are at equilibrium (i.e., the intersection between multiple reaction curves in PT space) and provides more robust PT estimates than using individual calculations for pressure and temperature.

It is necessary to consider the effects of reequilibration and retrograde net transfer reactions on garnet, biotite, and plagioclase element compositions when calculating peak PT estimates (e.g., Frost and Chacko, 1989; Kohn and Spear, 2000).

²Supplemental File 2. Description of methods used during data acquisition and analytical conditions for both major element analyses. Please visit <http://dx.doi.org/10.1130/GES01246.S2> or the full-text article on www.gsapubs.org to view Supplemental File 2.

³Supplemental File 3. Microprobe analysis data sets. Please visit <http://dx.doi.org/10.1130/GES01246.S3> or the full-text article on www.gsapubs.org to view Supplemental File 3.

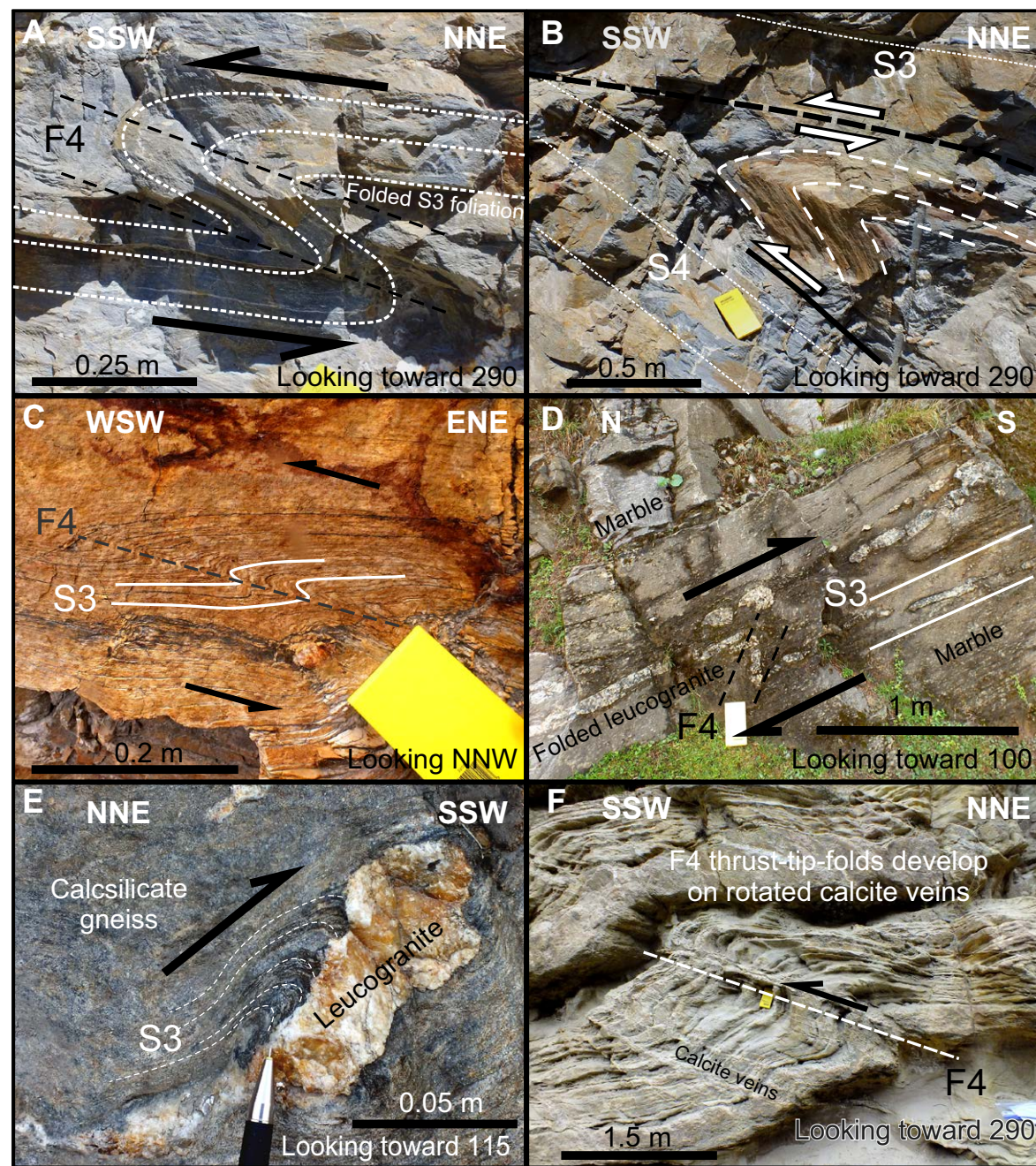


Figure 8. Top-SW shortening in the South Tibetan detachment system (STDS) and Tethyan Himalayan Sequence (THS), Kali Gandaki transect. See Plate 1 for locations of photographs. (A–C) F4 folding and associated top-S/SW shearing deform S3 foliation in the STDS. F4 hinge planes (dashed lines) are subparallel to S4 foliation. (D) Folded and boudinaged leucogranite in the STDS recording top-S shearing. Boudins appear to be shortened parallel to the shear direction, suggesting that they formed prior to top-to-the-S shearing. (E) Top-to-the-S shearing of S3 foliation on the margin of a leucogranite intrusion in the STDS, suggesting that reverse-sense shearing occurred after leucogranite emplacement. (F) F4 thrust-tip folding in the THS. S4-related compression has rotated preexisting calcite veins during top-S F4 thrust and fold development.

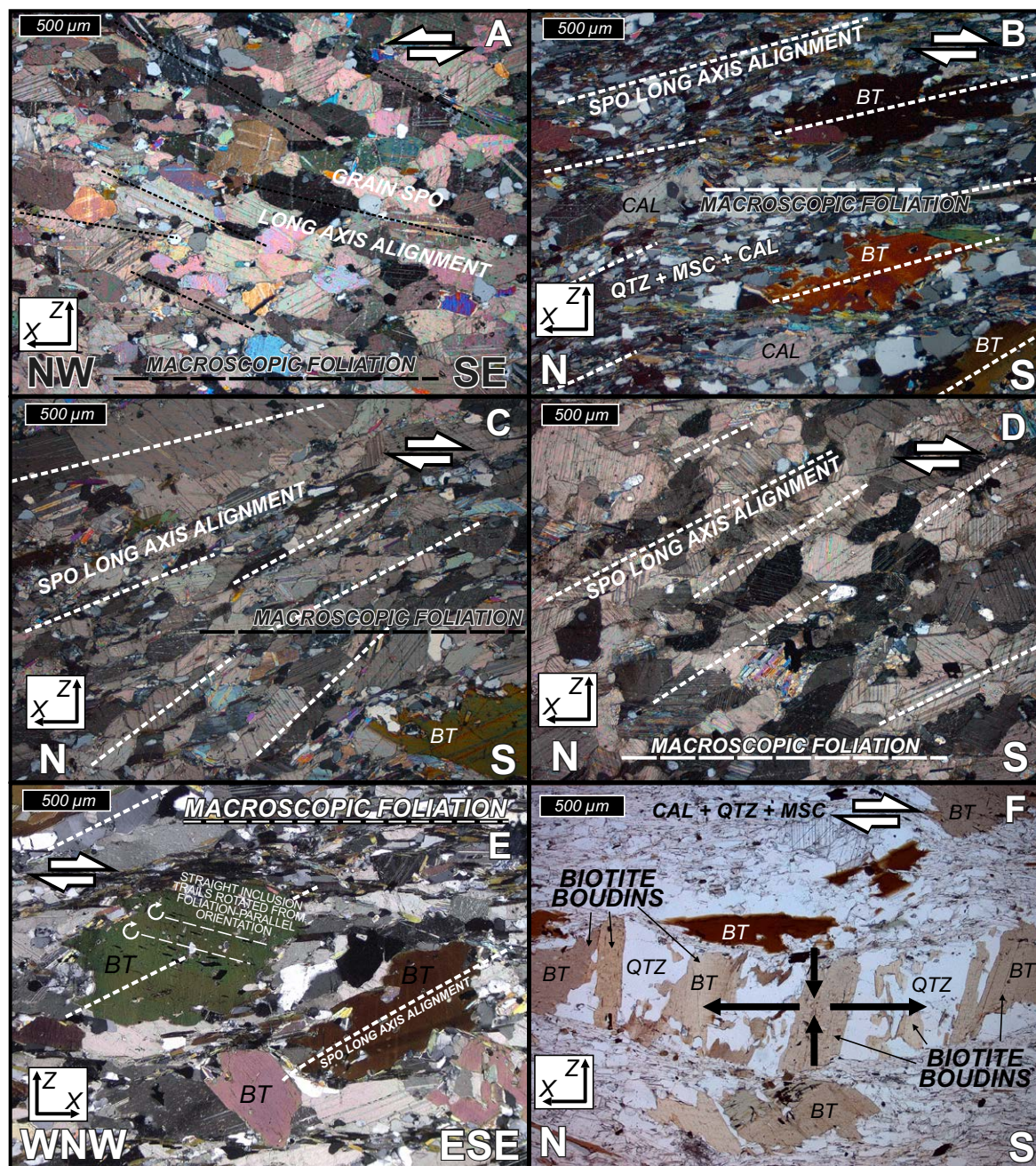


Figure 9. Microstructural shear-sense indicators in the South Tibetan detachment system (STDS)—Kali Gandaki. See Plate 1 and Figure 4 for relative structural positions of samples. (A) Sample P13/026—Grain-shape-preferred orientation (SPO) long-axis alignment of calcite and dolomite records top-NW (normal) sense at the base of the STDS. (B) Sample P13/008—Grain SPO long-axis alignment of calcite, quartz, and mica matrix grains and biotite (BT) porphyroblasts records top-S (reverse) sense shear from top of the STDS. (C) P13/008—Grain SPO long-axis alignment of calcite records top-S (reverse) sense shear from top of the STDS. (D) Sample P13/006—Grain-shape elongation of calcite records top-S (reverse) sense shear from the footwall of the STD. (E) Sample P12/044—Grain SPO long-axis alignment of biotite (BT) porphyroblasts records top-ESE (normal) sense shear. Straight inclusion trails in biotite record a dextral rotation relative to the foliation. (F) Sample P13/008—Boudinage of biotite porphyroblast. Quartz infills gaps between boudins.

Peak mineral compositions were determined using the methods outlined by Kohn et al. (1992), Dasgupta et al. (2004), and Corrie and Kohn (2011) (see Supplemental File 2 [footnote 2] for method details). Samples P12/055, P12/058, and P12/060 produced peak temperature estimates of 747 ± 10 °C, 703 ± 13 °C, and 688 ± 19 °C, respectively (Table 2). These samples respectively yielded peak pressure estimates of 11.4 ± 0.9 kbar, 11.5 ± 1.3 kbar, and 11.3 ± 1.2 kbar.

Four samples of calc-silicate gneiss (P12/053; P12/054–Unit II; P13/032–Unit III; P13/031–STDS; see Plate 1 for sample locations) were selected for Zr-in-titanite thermometry (Table 3). All samples contained calcite, zircon, quartz, and rutile (see Table 3 for full mineral assemblage of each sample). Samples P13/031 and P13/032 were sampled from immediately above and below the AD, respectively (Plate 1). Temperatures were calculated using the Zr-in-titanite thermometer of Hayden et al. (2008) from average titanite Zr concentrations (ppm) in individual samples. The highest temperatures in P12/053 were calculated from rim concentration of Zr and are assumed to reflect peak metamorphic conditions (Kohn and Corrie, 2011). Titanite rim and core temperatures from P13/031 and P13/032 were within error of each other and only titanite core temperatures were calculated for P12/054. These may reflect crystallization temperatures rather than peak metamorphic temperatures and thus provide a minimum bound for peak metamorphic conditions. For a pressure of 11 ± 1 kbar (based on GASP barometry from this study, plus Corrie and Kohn, 2011; laccarino et al., 2015), peak temperature

estimates of 740 ± 35 °C, 772 ± 33 °C, 744 ± 38 °C, and 720 ± 48 °C are calculated for samples P12/053, P12/054, P13/032, and P13/031, respectively (Table 3).

Our GARB-GASP thermobarometry results are similar to the results of laccarino et al. (2015), who record peak temperatures and pressures of 710–720 °C and 10–11 kbar from multi-equilibrium thermobarometry and Zr-in-rutile thermometry of a kyanite-migmatite in Unit I in the Kali Gandaki transect (Fig. 10A). Our Zr-in-titanite thermometry results from Unit II, Unit III, and the STDS are similar to previous temperature estimates from Unit II and Unit III in the Modi Khola valley (750–850 °C, Fig. 10B; Martin et al., 2010; Corrie and Kohn, 2011). Differences in results between this study and Le Fort et al. (1986) and Vannay and Hodges (1996) most likely derive from the use of different analytical procedures and thermobarometric calibrations to those used in this study. Vannay and Hodges (1996) analyzed the rims of garnet-biotite and garnet-plagioclase grain pairs that were in contact with each other, in accordance with the methods of Hodges and McKenna (1987) and Hodges et al. (1993). As stated by Vannay and Hodges (1996) and Hodges et al. (1993), the purpose of their employed analytical method was to determine the temperature and pressure at which these minerals equilibrated for the last time, and this is unlikely to yield PT estimates representative of peak conditions. Le Fort et al. (1986) also use different thermobarometers, and it is not clear what analytical methods they used to select element compositions for PT calculations.

TABLE 2. REPRESENTATIVE MINERAL ANALYSES (wt%) FOR GARNET, BIOTITE, AND PLAGIOCLASE AND THERMOBAROMETRY RESULTS

| Sample | Mineralogy | Mineral | SiO ₂ | TiO ₂ | Al ₂ O ₃ | Cr ₂ O ₃ | FeO | MnO | MgO | CaO | BaO | Na ₂ O | K ₂ O | F | Total | Temperature (°C) | Pressure (kbar) | |
|--|--|--|------------------|------------------|--------------------------------|--------------------------------|-------|------|-------|------|------|-------------------|------------------|------|----------|------------------|-----------------|------------|
| P12/055 | Qtz + Bt + Grt + Plg + Ky + Msc (secondary) + Rt | Biotite | 35.41 | 2.43 | 17.48 | 0.04 | 17.77 | 0.06 | 10.80 | 0.01 | 0.06 | 0.21 | 9.23 | 0.37 | 93.87 | — | — | |
| | | Plagioclase | 59.77 | 0.00 | 25.89 | 0.00 | 0.03 | 0.00 | 0.00 | 7.31 | 0.00 | 7.60 | 0.12 | 0.00 | 100.66 | — | — | |
| | | Garnet 1 | 37.86 | 0.02 | 21.33 | 0.02 | 29.97 | 1.31 | 4.89 | 4.78 | — | 0.00 | 0.00 | — | 100.18 | 747 | 11.4 | |
| | | Sample average temperature + pressure: | | | | | | | | | | | | | | | 747 ± 10 | 11.4 ± 0.9 |
| | | Mineral | SiO ₂ | TiO ₂ | Al ₂ O ₃ | Cr ₂ O ₃ | FeO | MnO | MgO | CaO | BaO | Na ₂ O | K ₂ O | F | Total | | | |
| P12/058 | Qtz + Bt + Grt + Plg (An% 0–30) + Ky + Rt | Biotite | 36.00 | 2.58 | 17.81 | 0.05 | 16.69 | 0.06 | 11.45 | 0.04 | 0.12 | 0.37 | 8.68 | 0.20 | 94.04 | — | — | |
| | | Plagioclase | 65.11 | 0.01 | 20.91 | 0.01 | 0.00 | 0.00 | 0.00 | 1.78 | 0.02 | 10.98 | 0.10 | 0.00 | 98.90 | — | — | |
| | | Garnet 1 | 38.10 | 0.00 | 21.46 | 0.01 | 32.62 | 1.32 | 6.09 | 0.95 | — | 0.02 | 0.00 | — | 100.58 | 707 | 11.7 | |
| | | Garnet 2 | 37.98 | 0.02 | 21.34 | 0.01 | 32.28 | 1.83 | 5.14 | 2.04 | — | 0.03 | 0.00 | — | 100.62 | 699 | 11.0 | |
| | | Garnet 3 | 38.00 | 0.00 | 21.63 | 0.00 | 32.84 | 1.15 | 6.04 | 1.01 | — | 0.03 | 0.00 | — | 100.70 | 703 | 11.8 | |
| | | Sample average temperature + pressure: | | | | | | | | | | | | | | | 703 ± 13 | 11.5 ± 1.3 |
| P12/060 | Qtz + Bt + Grt + Plg + Msc + Ilm | Mineral | SiO ₂ | TiO ₂ | Al ₂ O ₃ | Cr ₂ O ₃ | FeO | MnO | MgO | CaO | BaO | Na ₂ O | K ₂ O | F | Total | | | |
| | | Biotite | 36.16 | 2.08 | 17.60 | 0.04 | 17.04 | 0.06 | 11.56 | 0.04 | 0.29 | 0.25 | 8.45 | 0.00 | 93.56 | — | — | |
| | | Plagioclase | 62.49 | 0.00 | 22.57 | 0.00 | 0.01 | 0.00 | 0.00 | 3.73 | 0.03 | 9.79 | 0.10 | 0.00 | 98.72 | — | — | |
| | | Garnet 1 | 37.98 | 0.00 | 21.46 | 0.03 | 31.55 | 1.50 | 5.20 | 2.80 | — | 0.02 | 0.00 | — | 100.54 | 698 | 11.7 | |
| | | Garnet 2 | 37.76 | 0.01 | 21.42 | 0.00 | 32.05 | 1.53 | 4.94 | 2.68 | — | 0.03 | 0.00 | — | 100.43 | 679 | 11.0 | |
| | | Garnet 3 | 37.83 | 0.00 | 21.45 | 0.00 | 32.21 | 1.54 | 4.95 | 2.68 | — | 0.00 | 0.00 | — | 100.64 | 678 | 11.0 | |
| | | Garnet 4 | 37.81 | 0.00 | 21.42 | 0.01 | 31.57 | 1.42 | 5.17 | 2.70 | — | 0.02 | −0.04 | — | 100.09 | 695 | 11.5 | |
| Sample average temperature + pressure: | | | | | | | | | | | | | | | 688 ± 19 | 11.3 ± 1.2 | | |

Note: Mineral compositions of each sample indicated. Oxygen units per mineral formula as follows: garnet = 24 O, biotite = 12 O, plagioclase = 8 O. Abbreviations for mineralogy: An—anorthite; Bt—biotite; Grt—garnet; Ilm—ilmenite; Ky—kyanite; Msc—muscovite; Plg—plagioclase; Rt—rutile.

TABLE 3. TITANITE ZIRCON CONCENTRATIONS (PPM) AND THERMOMETRY RESULTS

| Unit | Mineralogy | Spot analysis | Rim or core | Zircon (ppm) | Temperature (°C) |
|--|--|---------------------------------------|-------------|--------------|------------------|
| UGHS Unit II | Ca + Qtz + Plg + Ksp + Scp + Clz + Tt + Cpx + Phl + Rt | P053_T2_2 | Rim | 91.92 | 740 |
| | | P053_T2_2 | Rim | 130.47 | 758 |
| | | P053_T2_2 | Rim | 108.92 | 748 |
| | | P053_T5_2 | Rim | 59.96 | 719 |
| | | P053_T7_2 | Rim | 85.84 | 736 |
| | | P053_T8_3 | Rim | 92.22 | 740 |
| | | P053_T8_3 | Rim | 84.56 | 736 |
| | | P053_T8_3 | Rim | 106.57 | 747 |
| | | P053_T9_2 | Rim | 108.31 | 748 |
| | | P053_T9_2 | Rim | 88.83 | 738 |
| | | P053_T9_2 | Rim | 73.04 | 728 |
| Sample average rim temperature (°C) | | | | | 740 ± 35 |
| | | Spot analysis | Rim or core | Zircon (ppm) | Temperature (°C) |
| UGHS Unit II | Ca + Qtz + Plg + Ksp + Scp + Clz + Tt + Cpx + Msc + Rt | P054_T1_1 | Core | 183.92 | 776 |
| | | P054_T1_1 | Core | 158.07 | 768 |
| | | P054_T2_1 | Core | 176.08 | 774 |
| | | P054_T2_1 | Core | 152.16 | 766 |
| | | P054_T3_1 | Core | 200.81 | 781 |
| | | P054_T3_1 | Core | 203.59 | 782 |
| | | P054_T6_1 | Core | 165.41 | 771 |
| | | P054_T8_1 | Core | 148.27 | 765 |
| | | P054_T8_1 | Core | 164.6 | 770 |
| | | P054_T9_1 | Core | 181.68 | 776 |
| | | P054_T9_3 | Core | 181.95 | 776 |
| | | P054_T10_1 | Core | 179.4 | 775 |
| | | P054_T10_1 | Core | 196.67 | 780 |
| | | P054_T16_1 | Core | 148.95 | 765 |
| | | P054_T16_1 | Core | 128.42 | 757 |
| | | Sample average core temperature (°C) | | | |
| | | Spot analysis | Rim or core | Zircon (ppm) | Temperature (°C) |
| UGHS Unit III | Ca + Qtz + Plg + Ksp + Scp + Clz + Tt + Bt + Rt | P032_T7_1 | Core | 141.76 | 762 |
| | | P032_T7_3 | Rim | 91.03 | 739 |
| | | P032_T11_2 | Rim | 90.53 | 739 |
| | | P032_T12_4 | Core | 132.75 | 759 |
| | | P032_T13_1 | Core | 87.87 | 737 |
| | | P032_T13_2 | Core | 96.69 | 742 |
| | | P032_T13_3 | Core | 108.11 | 748 |
| | | P032_T13_4 | Rim | 62.41 | 720 |
| | | Sample average grain temperature (°C) | | | |
| | | Spot analysis | Rim or core | Zircon (ppm) | Temperature (°C) |
| STDS | Ca + Qtz + Plg + Ksp + Scp + Clz + Tt + Cpx + Amp + Grt + Rt | P031_T3_1 | Core | 69.58 | 726 |
| | | P031_T3_3 | Rim | 87.71 | 737 |
| | | P031_T6_1 | Core | 42.34 | 702 |
| | | P031_T8_3 | Rim | 56.41 | 716 |
| | | P031_T10_2 | Core | 137.62 | 761 |
| | | P031_T12_1 | Core | 35.56 | 694 |
| | | P031_T12_4 | Rim | 31.14 | 688 |
| | | P031_T13_1 | Core | 108.28 | 748 |
| | | P031_T15_1 | Core | 44.92 | 705 |
| Sample average grain temperature (°C) | | | | | 720 ± 48 |
| Note: Abbreviations: Amp—amphibolite; Bt—biotite; Ca—calcium; Clz—clinozoisite; Cpx—clinopyroxene; Grt—garnet; Ksp—K-feldspar; Msc—muscovite; Plg—plagioclase; Rt—rutile; Scp—scapolite; Tt—titanite; STDS—South Tibetan detachment center; UGHS—Upper Greater Himalayan Sequence. | | | | | |

Note: Abbreviations: Amp—amphibolite; Bt—biotite; Ca—calcium; Clz—clinozoisite; Cpx—clinopyroxene; Grt—garnet; Ksp—K-feldspar; Msc—muscovite; Plg—plagioclase; Rt—rutile; Scp—scapolite; Tt—titanite; STDS—South Tibetan detachment center; UGHS—Upper Greater Himalayan Sequence.

4. ATYPICAL GEOLOGICAL FEATURES OF THE ANNAPURNA-DHAULAGIRI HIMALAYA AND THEIR KINEMATIC-DYNAMIC IMPLICATIONS

The GHS in the Annapurna-Dhaulagiri Himalaya differs from more typical GHS sections elsewhere (e.g., Everest-Makalu Himalaya and Sikkim Himalaya) upon which the channel-flow model was based, with atypically low volumes of leucogranite and migmatite, an absence of evidence for partial melting within the sillimanite stability field, a smaller structural thickness (<10 km), and evidence for late-stage top-SW shortening on the STDS (Brown and Nazarchuk, 1993; Nazarchuk, 1993; Hodges et al., 1996; Godin et al., 1999a; Godin, 2003; Larson and Godin, 2009; Parsons et al., 2016). Additionally, alternative models of underplating and thrust stacking or composite channel-flow–underplating models have been proposed for mid-crustal emplacement of the GHS in the Annapurna-Dhaulagiri Himalaya, following identification of several metamorphic discontinuities within the GHS (Martin et al., 2010; Corrie and Kohn, 2011; Montomoli et al., 2015; see review by Cottle et al., 2015). These atypical features and their implications for applicability of the channel-flow model and kinematic evolution of the Annapurna-Dhaulagiri Himalaya are discussed and assessed below.

4.1. Reduced Volumes of Leucogranite and Migmatite and Absence of Evidence for Partial Melting within the Sillimanite Stability Field

A key feature in the structure of the GHS observed along the length of the Himalaya is a high concentration of leucogranite dikes, sills, and injection complexes throughout UGHS- and STDS-equivalent structural sections. These melt-bearing sections typically have maximum combined thicknesses of tens to thousands of meters and can account for >50% of the total volume of UGHS-equivalent sections (e.g., Garhwal—Scaillet et al., 1990; Langtang—Inger and Harris, 1992; Bhutan—Grujic et al., 1996; Manaslu—Harrison et al., 1999; Zaskar—Walker et al., 1999; Everest—Searle et al., 2003; Sikkim—Searle and Szulc, 2005; Makalu—Streule et al., 2010). Typically, most partial melts and leucogranites are the product of fluid-absent muscovite dehydration and, at higher temperatures and lower pressures, biotite dehydration. These reactions occurred during isothermal to near-isothermal exhumation of the UGHS from high-temperature–high-pressure (>700 °C, 8–14 kbar) to high-temperature–low-pressure (>700 °C, 2–6 kbar) conditions (Fig. 11) (Harris and Massey, 1994; Guillot et al., 1999; Visonà and Lombardo, 2002; Searle et al., 2010; Streule et al., 2010). This exhumation corresponds to the Neohimalayan M2 metamorphic event that is reported from across the orogen within the sillimanite stability field between 22 and 15 Ma and is coincident with activity on the MCT and STD (Guillot et al., 1999; Searle et al., 2010). Importantly, if melt production continued during exhumation, the melt-weakened rheology (i.e., low viscosity) of the UGHS should have allowed crustal flow to continue to lower pressures during exhumation (Beaumont et al., 2004; Jamieson et al., 2004).

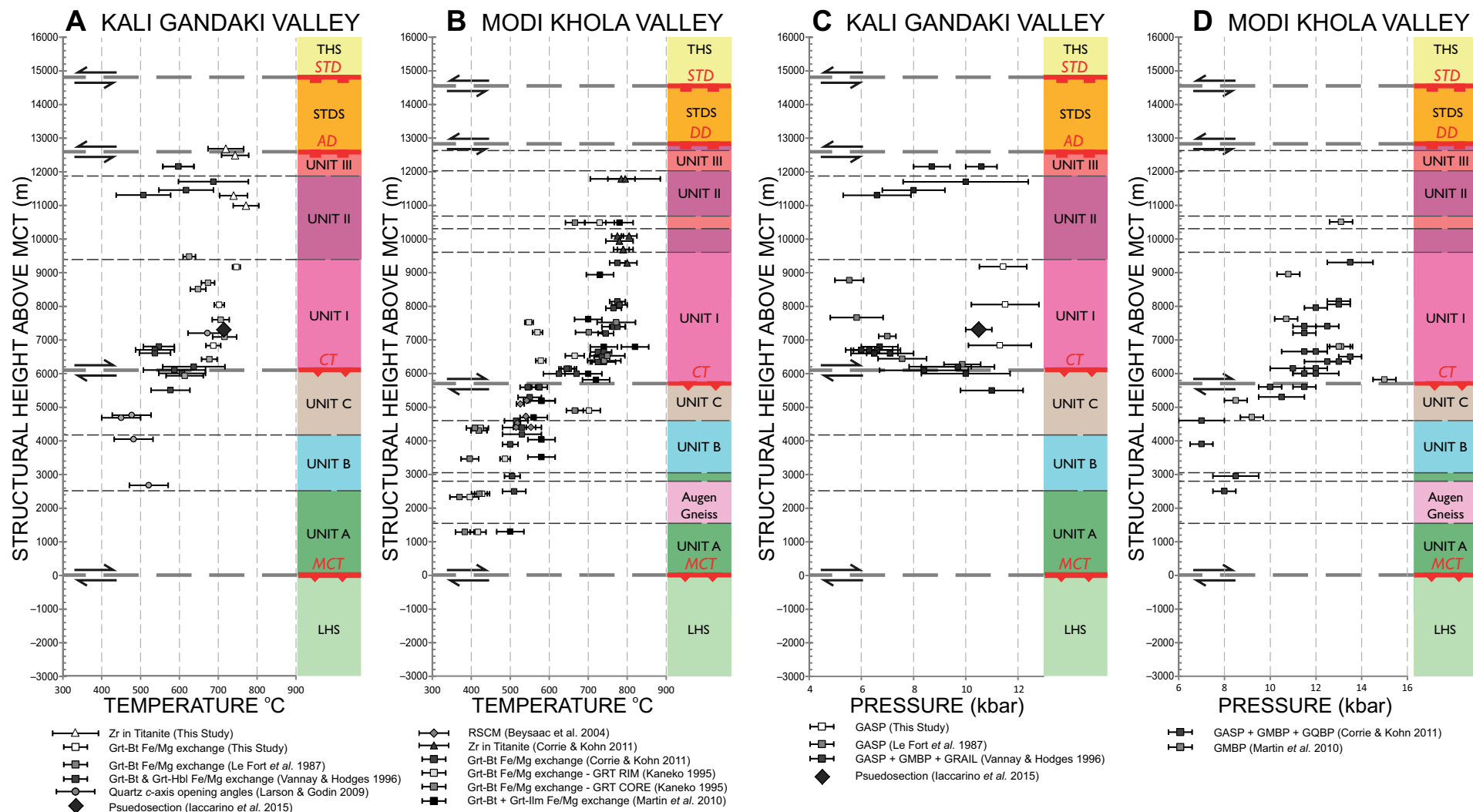


Figure 10. Variation in estimated temperatures and pressures of metamorphism (mainly peak) and quartz deformation in the Greater Himalayan Sequence (GHS) with structural distance above the Main Central thrust (MCT). Locations of all data points plotted to scale at relative structural distance above the MCT. Lithotectonic units plotted to scale to the right of each profile. (A) Thermal profile for the GHS in the Kali Gandaki valley, with new thermometric constraints produced from this study (white markers) and previously published constraints (gray to black markers). (B) Thermal profile for the GHS in the Modi Khola valley, based on previously published data. (C) Pressure profile for the GHS in the Kali Gandaki valley, with new barometric constraints produced from this study (white markers) and previously published constraints (gray to black markers). (D) Pressure profile for the GHS in the Modi Khola valley, based on previously published data. See figure for data sources. Abbreviations as follows: Bt—biotite; GASP—garnet-aluminosilicate-silica-plagioclase; GMBP—garnet-muscovite-biotite-plagioclase; GQBP—garnet-quartz-biotite-plagioclase; GRAIL—garnet-rutile-aluminosilicate-ilmenite-quartz; Grt—garnet; Ilm—ilmenite; RSCM—Raman spectroscopy of carbonaceous material.

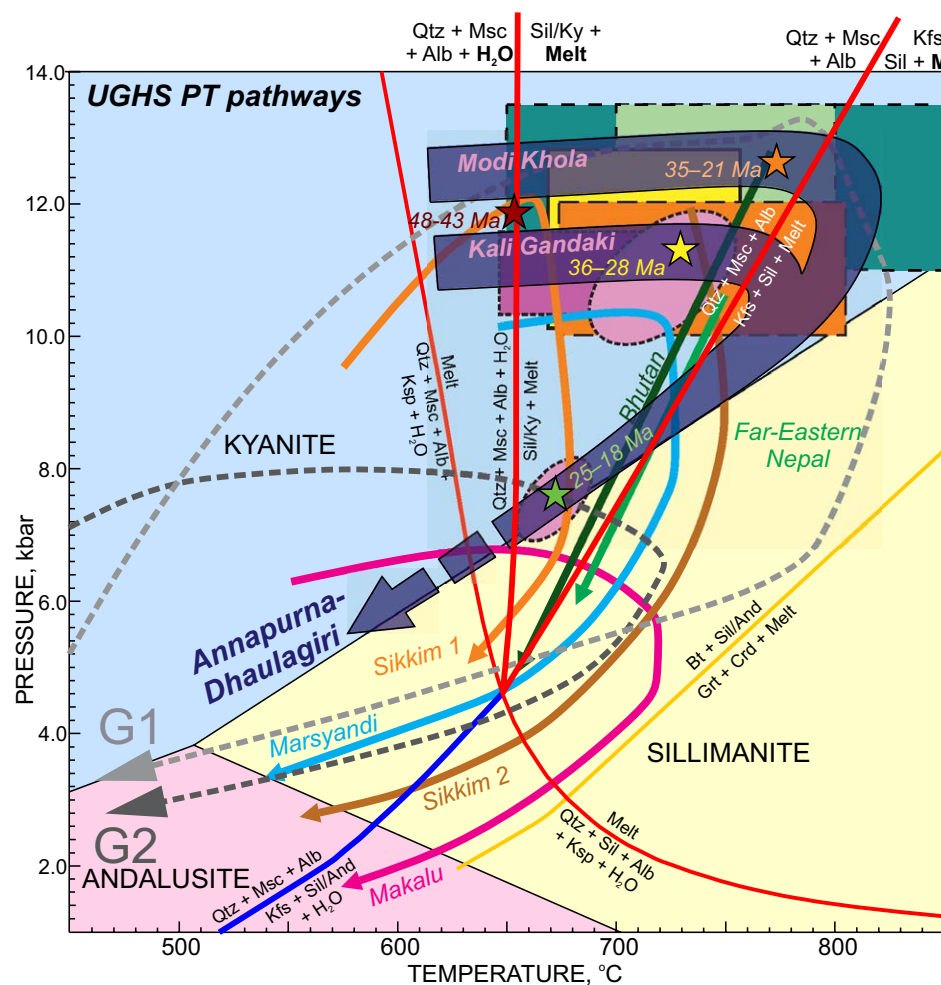


Figure 11. Summary of pressure-temperature (PT) pathways for the Upper Greater Himalayan Sequence (UGHS) across the Himalayan orogen. Light-orange PT path—Sikkim 1 section, Harris et al., 2004; dark-orange PT path—Sikkim 2 section, Mottram et al., 2015; light-blue PT path—Marsyandi section, Caddick, 2005; magenta PT path—Makalu section, Streule et al., 2010; light-green PT path—Far-Eastern Nepal section, Imai et al., 2012; dark-green PT path—Bhutan section, Daniel et al., 2003. Thick, semi-transparent, purple PT path represents proposed PT pathway for the UGHS of the Annapurna-Dhaulagiri Himalaya based on petrologic observations and thermobarometric constraints from this study in addition to Le Fort et al., 1986; Pêcher, 1989; Hodges et al., 1996; Godin et al., 2001; Martin et al., 2010; Corrie and Kohn, 2011; Kohn and Corrie, 2011; Carosi et al., 2015; and Iaccarino et al., 2015. Colored squares and ellipses show PT constraints from this study (garnet-biotite cation exchange–garnet–aluminosilicate–silica–plagioclase [GAR-B-GASP]—yellow box, Zr-in-titanite—orange box; Martin et al., 2010 and Corrie and Kohn, 2011 (dark green box); Kohn and Corrie, 2012 (light green box) and Iaccarino et al., 2015 (purple box—Zr-in-rutile; pink ellipses—pseudo-section results). Colored stars indicate timing of initiation of prograde metamorphism (red star), peak metamorphism in the Modi Khola section (orange star), peak metamorphism in the Kali Gandaki section (yellow star), and retrograde metamorphism in the Kali Gandaki section (green star). See text for geochronometry sources. Dashed gray lines (G1 and G2) show pressure-temperature-time (PTt) particle paths from thermomechanical channel-flow model HT1 (Jamieson et al., 2004). Reaction curves derived from White et al. (2001) and Visonà and Lombardo (2002).

In the Annapurna-Dhaulagiri Himalaya, leucogranite bodies are no larger than tens of meters in thickness, and injection complexes are only observed in the Modi Khola transect and are less densely packed with dikes and sills than typically observed in other regions (Nazarchuk, 1993; Hodges et al., 1996; Larson and Godin, 2009). Leucosome content within migmatites ranges between 5% and 20% in the Kali Gandaki valley and 10%–40% in the Modi Khola valley, which is comparable to observations recorded elsewhere in the Himalaya that record ~10%–40% partial melting within the GHS (e.g., Inger and Harris, 1992; Harris et al., 2004; Larson et al., 2010). However, migmatite volume within the UGHS is comparatively low and accounts for <50% of the structural thickness

of Unit I, confined to ≤50-m-thick horizons and is almost negligible in Unit II and Unit III. Elsewhere in the Himalaya, UGHS-equivalent migmatitic sections can be as much as 10 km thick (Searle, 2013).

Pressure-temperature-time (PTt) constraints from the lower portion of the UGHS in the Annapurna-Dhaulagiri Himalaya indicate that burial and heating at kyanite-grade conditions (Fig. 11) initiated at ca. 48–43 Ma (Carosi et al., 2015; Iaccarino et al., 2015; Larson and Cottle, 2015). Subsequently, partial melting initiated as early as 41 Ma (Carosi et al., 2015) and continued almost entirely within the kyanite stability field to as late as 18.5 Ma (Nazarchuk, 1993; Hodges et al., 1996; Godin et al., 2001; Martin et al., 2010; Cottle et al., 2011; Kohn and

Corrie, 2011; Carosi et al., 2015; Iaccarino et al., 2015; Larson and Cottle, 2015). As such, it is possible that melt volumes within the UGHS were not always low. If lateral melt migration occurred during deformation, then melt volumes in the exposed UGHS may not directly correspond to the amount of partial melting, especially if melt migration out-paced melt production. However, melt migration observed in the GHS across the Himalaya is dominantly vertical (up-section) (e.g., Harris and Massey, 1994; Hodges et al., 1996). There is no direct evidence of lateral melt migration in the Annapurna-Dhaulagiri Himalaya, although such phenomena are not ruled out.

It is acknowledged that the PTt evolution of different structural positions in the UGHS may vary (Jamieson et al., 2004; Cottle et al., 2015). However, available constraints suggest that the PTt evolution of the upper portion of the UGHS in the Annapurna-Dhaulagiri Himalaya (Fig. 10, Godin et al., 2001; Corrie and Kohn, 2011) may not be that different from the lower portion. In the upper portion of the UGHS, peak temperature metamorphism and associated in situ partial melting are recorded at 35–30 Ma (Godin et al., 2001; Corrie and Kohn, 2011). Leucogranite dikes with crystallization ages of 23–18.5 Ma are also identified from the STDS and upper UGHS (Hodges et al., 1996; Godin et al., 2001). These ages may indicate that partial melting initiated earlier in the lower portion of the UGHS (41 Ma) than in the upper portion (35 Ma) and the STDS. Alternatively, they may imply that multiple phases of melting and crystallization occurred between 41 and 18 Ma.

Field and petrological observations indicate that partial melting and leucogranite production occurred within the kyanite stability field (Hodges et al., 1996; Godin et al., 2001; Corrie and Kohn, 2011; Carosi et al., 2015; Iaccarino et al., 2015; Larson and Cottle, 2015). Evidence for partial melting within the sillimanite stability field is absent, and leucosomes observed within the upper portion of the UGHS contain kyanite, not sillimanite, and remain low in volume (Nazarchuk, 1993; Hodges et al., 1996; Godin et al., 2001; Corrie and Kohn, 2011; Parsons et al., 2016). Where present, sillimanite is identified as a late-stage overgrowth postdating partial melting under lower temperature retrograde conditions (Carosi et al., 2015; Iaccarino et al., 2015). Consequently, it is unlikely that the PTt path for the UGHS entered the sillimanite stability field at high temperatures and may have only resided there for a short period of time during retrogression (Carosi et al., 2015; Iaccarino et al., 2015). The available PTt constraints (Figs. 10 and 11) suggest that exhumation of the UGHS in the Annapurna-Dhaulagiri Himalaya followed a much shallower PTt path (this study; Pêcher, 1989; Iaccarino et al., 2015) than recorded elsewhere in the Himalaya (Fig. 11). Isothermal decompression was not a characteristic feature of metamorphism in this region and explains the reduced volumes of sillimanite-bearing metapelitic rocks and the absence of partial melting in the sillimanite stability field in the Annapurna-Dhaulagiri Himalaya. Isothermal decompression requires rapid exhumation that out-paces rates of cooling so that high temperatures are maintained through to lower pressures (Whitney et al., 2004). Consequently, a less steep exhumation path (i.e., non-isothermal) suggests that the UGHS in the Annapurna-Dhaulagiri Himalaya either exhumed slower or cooled faster relative to equivalent UGHS sections with isothermal

exhumation paths. Given the lack of potential explanations for faster cooling, we propose that the shallow gradient exhumation path of the UGHS is indicative of slower exhumation.

The shallow gradient of the PTt exhumation path also suggests that fluid-absent muscovite dehydration may have only occurred during the initial phase of exhumation, while biotite dehydration could not occur at any stage during exhumation, which may have contributed further to the apparently low volumes of melt produced during exhumation. Lateral melt migration out-pacing melt production would also account for the low melt volumes.

4.2. Viscosity of the UGHS during Peak Metamorphism

Widespread partial melting is the proposed mechanism for the viscosity reduction needed to initiate and sustain mid-crustal channel flow during the Himalayan orogeny (Beaumont et al., 2001, 2004; Grujic, 2006; Rosenberg et al., 2007; Jamieson et al., 2011). While the volume of migmatite and leucogranite in the Annapurna-Dhaulagiri Himalaya is lower than elsewhere in the Himalaya, metamorphic and geochronometric constraints suggest that temperatures and melt volumes may still have been high enough for mid-crustal flow during peak conditions prior to the onset of exhumation.

At a given temperature (T) and flow stress (σ), the visco-plastic creep of geological materials is defined (e.g., Passchier and Trouw, 2005) by a flow law of the form:

$$\dot{\epsilon} = A\sigma^n \exp(-Q/RT), \quad (1)$$

where strain rate, $\dot{\epsilon}$, is controlled by a pre-exponential constant A ($\text{MPa}^{-n} \text{s}^{-1}$), the power-law stress exponent, n , activation energy, Q (kJ mol^{-1}), and gas constant, R . Table 4A lists the experimentally derived flow law parameters for Blackhill quartzite (wet, 0.15 wt% H_2O) with small amounts (1%–2%) of melt (Gleason and Tullis, 1995), Heavitree quartzite (dry) (Jaoul et al., 1984), Westerly granite (dry) (Hansen and Carter, 1983), and Maryland diabase (dry) (Caristan, 1982). Additionally, a modified flow law for experimentally deformed partially molten synthetic granite (Table 4B) is given by Rutter et al. (2006):

$$\dot{\epsilon} = A \exp(B\Phi^m) \exp(-Q/RT) \sigma^n, \quad (2)$$

where Φ is the melt fraction, ranging from 0 (0% melt) to 1 (100% melt), and B and m are material constants. Together, we use these flow laws as proxies for the rheologies of quartzite and quartzofeldspathic gneiss (Blackhill quartzite, Heavitree quartzite, and Westerly granite flow laws), calc-silicate gneiss (Maryland diabase flow law), and migmatite (partially molten synthetic granite flow law), which respectively represent ~35%–70%, ~30%–40%, and <35% volume of the UGHS in the Annapurna-Dhaulagiri Himalaya. It is noted that none of the flow laws presented account for rocks with high percentage volumes of mica. The development of interlocking crystal textures during high-temperature

TABLE 4A. FLOW-LAW–DERIVED STRAIN RATE ($\dot{\epsilon}$) AND VISCOSITY (μ) ESTIMATES AT FLOW STRESSES (σ) OF 10 MPa AND 2 MPa

| | A (MPa $^{-n}$ s $^{-1}$) | Q (kJ mol $^{-1}$) | n | σ (MPa) | $\dot{\epsilon}$ (s $^{-1}$) | μ (Pa s) | Source |
|---|---------------------------------|--------------------------|-----------------|-------------------|----------------------------------|----------------------|-----------------------------|
| Blackhill quartzite with melt (0.15 wt% H ₂ O) | 1.80×10^{-08} | 137 ± 34 | 4 ± 0.9 | 10 | 1.8×10^{-11} | 5.5×10^{17} | Gleason and Tullis, 1995 |
| | | | | 2 | 2.9×10^{-14} | 6.9×10^{19} | |
| Heavtree quartzite (vacuum dried) | 3.44×10^{-06} | 184 ± 6 | 2.8 ± 0.2 | 10 | 8.8×10^{-13} | 1.1×10^{19} | Jaoul et al., 1984 |
| | | | | 2 | 9.7×10^{-15} | 2.1×10^{20} | |
| Westerly granite (dry) | 2.00×10^{-06} | 186.5 | 3.3 | 10 | 1.2×10^{-12} | 8.3×10^{18} | Hansen and Carter, 1983 |
| | | | | 2 | 5.9×10^{-15} | 4.7×10^{20} | |
| Maryland diabase (dry) | 6.31×10^{-02} | 276 ± 14 | 3.05 ± 0.15 | 10 | 5.8×10^{-13} | 1.7×10^{19} | Caristan, 1982 |
| | | | | 2 | 4.3×10^{-15} | 4.7×10^{20} | |

Note: Flow-law parameters for selected geological materials are presented. A —pre-exponent constant, Q —activation energy, n —power-law exponent (see text for citations).

TABLE 4B. STRAIN RATE ($\dot{\epsilon}$) AND VISCOSITY (μ) DERIVED FROM A MODIFIED FLOW LAW FOR PARTIALLY MOLTEN SYNTHETIC GRANITE

| | A (MPa $^{-n}$ s $^{-1}$) | Q (kJ mol $^{-1}$) | n | m | B | ϕ | σ (MPa) | $\dot{\epsilon}$ (s $^{-1}$) | μ (Pa s) |
|---|---------------------------------|--------------------------|-----|-----|-----|--------|-------------------|----------------------------------|----------------------|
| Partially molten synthetic granite Rutter et al., 2006 | 4.07×10^{-02} | 230 ± 66 | 1.8 | 3 | 192 | 0.1 | 10 | 1.8×10^{-11} | 5.5×10^{17} |
| | | | | | | | 2 | 1.0×10^{-12} | 2.0×10^{18} |
| | | | | | | 0.2 | 10 | 7.0×10^{-11} | 1.4×10^{17} |
| | | | | | | | 2 | 3.9×10^{-12} | 5.2×10^{17} |
| | | | | | | 0.3 | 10 | 2.7×10^{-09} | 3.7×10^{15} |
| | | | | | | | 2 | 1.5×10^{-10} | 1.4×10^{16} |

Abbreviations: A —pre-exponent constant, B and m —post-exponent constants, Q —activation energy, n —power-law exponent, ϕ —melt fraction (from Rutter et al., 2006).

dynamic recrystallization typically strengthens a rock. Increased mica content can hinder these recrystallization processes and may result in a weaker rheology (e.g., Passchier and Trouw, 2005). However, most rocks from the UGHS form interlocking frameworks of quartz and feldspar grains that control strength and rheological behavior (e.g., Handy, 1990).

The equation,

$$\mu = \sigma / \dot{\epsilon}, \quad (3)$$

allows the flow laws (Equations 1 and 2) to be used to estimate the viscosity, μ , of the UGHS during peak metamorphism (Table 4). Temperature ($T = 750$ °C) is determined from peak metamorphic constraints from the UGHS in both the Kali Gandaki and Modi Khola valleys. A flow stress (σ) of 10 MPa is assumed, based on values calculated using the quartz recrystallized piezometer for UGHS-equivalent rocks in NW India (Law et al., 2013). Viscosity calculations are also made for an assumed flow stress of 2 MPa, to account for reduced flow stresses predicted in the center of a channel flow (Grujic, 2006). Observations from migmatitic sections in the UGHS of the Annapurna-Dhaulagiri Himalaya typically record melt fractions (Φ) of ~0.1–0.3 (i.e., 10%–30%).

For a flow stress of ~10 MPa, most of the flow laws yield viscosities (Table 4) that are equal to or lower than the “melt-weakened” viscosity (10^{19} Pa s) re-

quired to numerically simulate mid-crustal channel flow (Beaumont et al., 2001). However, at lower flow stresses ($\sigma = 2$ MPa) that may be more representative of conditions toward the center of the channel (Grujic et al., 1996; Grujic, 2006; Law et al., 2013), all melt-free flow laws except for Blackhill quartzite yield a viscosity of 10^{20} Pa s (Table 4). Additionally, Fourier transform infrared spectroscopy of quartzites from UGHS-equivalent strata in the Sutlje valley of NW India records remarkably low volumes of water (Kronenberg et al., 2014) and suggests that the Heavtree (dry) quartzite flow law should be favored over the Blackhill (wet) quartzite flow law. The flow law for a partially molten synthetic granite, which we use as a proxy for migmatite rheology, yields very low viscosities even at low flow stresses. However, migmatites account for <35% of the UGHS structural thickness and are present in relatively thin bands (<50 m thick). As such, while this flow law clearly demonstrates the rheological weakening effect caused by partial melting, it is not representative of the bulk volume of the UGHS. Instead, the rheology of the UGHS is more likely to have been controlled by the major load-bearing lithologies that account for >65% of its structural thickness (i.e., quartzofeldspathic and calc-silicate gneisses). Viscosity estimates for these lithologies toward the center of the channel are on the order of 10^{20} Pa s, which is an order of magnitude greater than the “melt-weakened” viscosity (10^{19} Pa s) simulated by model HT1 of Beaumont et al. (2004).

An additional constraint on flow conditions for the UGHS during its mid-crustal evolution is structural (i.e., channel) thickness (Beaumont et al., 2004; Jamieson et al., 2004; Mukherjee, 2013a). A reduction in channel thickness increases the effective viscosity of the channel material and results in a reduction of the threshold viscosity below which return flow in a hybrid channel flow may occur (Turcotte and Schubert, 2002; Grujic, 2006). The numerically modeled thickness required for a southward-directed return flow to develop in the HT1 model is ~10–20 km (Beaumont et al., 2004; Jamieson et al., 2004). In most regions, UGHS-equivalent strata match or exceed this thickness (e.g., 10–15 km—Bhutan, Manaslu, Garhwal [Grujic et al., 2002; Searle and Godin, 2003; Webb et al., 2011]; 20 km—Langtang, Sikkim [Inger and Harris, 1992; Searle and Szulc, 2005]; 30 km—Everest-Makalu [Searle et al., 2003; Jessup et al., 2006; Streule et al., 2010]). However, the UGHS of the Annapurna-Dhaulagiri Himalaya has a structural thickness of only ~7 km and consequently, it is necessary to consider whether this reduced thickness would hinder or even prevent the development of a hybrid channel flow with a southward-directed return flow component (Godin et al., 2006a).

Rearranging equation 6-17 of Turcotte and Schubert (2002) allows the relationship between channel viscosity (μ) and channel thickness (h) to be explored,

$$\mu = - \left[\frac{1}{12} \left\{ \frac{h^2}{\left(u_m - (u_0/2) \right) \frac{dp}{dx}} \right\} \right] \quad (4)$$

The average channel velocity (u_m) of the down-going channel wall (u_0) and horizontal pressure gradient (dp/dx , where dp is the difference in channel pressure over the horizontal channel distance, dx) must also be known, and a linear viscous rheology is assumed (Turcotte and Schubert, 2002). Suitable parameters may be derived from the return-flow portion of four particle pathways (G1–G4, Table 5) taken from thermomechanical channel-flow model HT1 of Beaumont et al. (2004) and Jamieson et al. (2004; their figure 4). Over a 24 m.y. period of southward-directed channel flow with a convergence rate of 50 mm yr⁻¹, the particle pathways from model HT1 have a time-averaged velocity of 0.017–0.018 m yr⁻¹ and undergo a 1.75–8.75 kbar reduction in pressure over a

horizontal distance of 416–430 km (Table 5). In order to maintain this velocity over this distance and pressure decrease, a modeled channel flow of 7 km thickness requires an estimated viscosity of 7.1×10^{18} to 3.7×10^{19} Pa s (Table 5). Larger viscosities would produce slower flow velocities, resulting in a more “sluggish” channel flow than that simulated by model HT1.

Assuming deformation was isochoric, transport-perpendicular shortening estimates of 25%–32% from the GHS in the Kali Gandaki valley (Larson and Godin, 2009) suggest that the UGHS may have had an initial thickness of 9.3–10.3 km. Larson and Godin (2009) state that their shortening estimates are likely to be underestimates. Larger shortening estimates of 35%–50% reported elsewhere in the Himalaya would indicate an initial thickness of up to 14 km (Larson et al., 2010; Law et al., 2013). If volume loss occurred during channel flow due to the lateral migration of magma, then the initial channel thickness may have been even greater. Using the HT1 channel-flow parameters defined above, the estimated viscosity of a larger channel thickness of 9–14 km must not exceed 1.25×10^{19} Pa s to 1.48×10^{20} Pa s in order to replicate the channel flow simulated by model HT1 (Table 5).

Assuming the chosen flow laws provide representative rheologies, much of the UGHS in the Annapurna-Dhaulagiri Himalaya, which consists of melt-free and probably dry quartzites and para-, ortho- and calc-silicate gneisses, was probably too viscous for channel flow to occur at modeled rates simulated by model HT1, if confined to a 7-km-wide channel with no change in channel thickness during flow. In order to maintain a constant channel thickness during channel flow, volume addition must occur to counteract transport-parallel shortening (e.g., Grasemann et al., 2006). Volume addition due to the migration and culmination of large leucogranite bodies and injection complexes is evident in UGHS-equivalent sections elsewhere along the Himalaya (e.g., Harrison et al., 1999; Grasemann et al., 2006; Searle et al., 2010; Searle, 2013). However, the absence of large leucogranite bodies and injection complexes in the Annapurna-Dhaulagiri Himalaya suggests that volume addition during channel flow of the UGHS in this region was negligible. Consequently, shortening estimates suggest that the UGHS may have been 9–14 km thick at the initial onset of channel flow. The possibility of volume loss due to lateral melt migration during channel flow implies that these are minimum initial thickness estimates.

TABLE 5. THRESHOLD VISCOSITY FOR FLOW, μ , FOR HYBRID CHANNEL FLOWS OF VARIABLE CHANNEL THICKNESSES, h , DETERMINED FROM EQUATION 4

| Particle path | Velocity (m yr ⁻¹) | Distance (km) | Time (t, m.y.) | Pressure (P0, kbar) | Pressure (P1 kbar) | Δ Pressure (kbar) | Threshold viscosity for flow, μ (Pa s) for channel thickness, h | | | |
|---------------|--------------------------------|---------------|----------------|---------------------|--------------------|--------------------------|---|-----------------------|-----------------------|-----------------------|
| | | | | | | | $h = 7$ km | $h = 9.3$ km | $h = 10.3$ km | $h = 14$ km |
| G1 | 0.018 | 430 | 24 | 13 | 4.25 | 8.75 | 3.70×10^{19} | 6.58×10^{19} | 8.00×10^{19} | 1.48×10^{20} |
| G2 | 0.018 | 422 | 24 | 8 | 3.75 | 4.25 | 1.75×10^{19} | 3.12×10^{19} | 3.79×10^{19} | 7.01×10^{19} |
| G3 | 0.017 | 420 | 24 | 6 | 3.75 | 2.25 | 9.19×10^{18} | 1.63×10^{19} | 1.99×10^{19} | 3.68×10^{19} |
| G4 | 0.017 | 416 | 24 | 4 | 2.25 | 1.75 | 7.07×10^{18} | 1.26×10^{19} | 1.53×10^{19} | 2.83×10^{19} |

Note: Channel-flow parameters derived from return flow portion of channel-flow particle pathways G1–G4, from thermomechanical channel-flow model HT1 (Jamieson et al., 2004). Threshold viscosities are maximum viscosities capable of replicating channel flow simulated by model HT1. See text for discussion.

At these larger initial thicknesses, many of the flow-law–derived viscosity estimates are of the same order of magnitude or lower than that required to produce flow velocities simulated by channel-flow model HT1 (Table 5). As such, these data suggest that prior to vertical shortening, the UGHS in the Annapurna-Dhaulagiri Himalaya was at least weak enough for mid-crustal channel flow to initiate. However, without the addition of new material during flow, as suggested by the absence of large culminations of leucogranite, the subsequent decrease in channel thickness due to vertical shortening resulted in a gradual increase in effective viscosity, which decelerated channel flow to slower rates than those predicted by both the thermomechanical models (Beaumont et al., 2001; Jamieson et al., 2004) and elsewhere in the Himalaya where melt content and structural thickness are typically higher. Being limited by a greater-than-typical viscosity, channel flow in the Annapurna-Dhaulagiri Himalaya may have been too viscous to facilitate isothermal exhumation. These calculations highlight the importance of volume addition during channel flow as a means of maintaining low viscosities.

4.3. Top-SW Shortening on the STDS

The STDS forms a top-NE shear zone at the top of the GHS that can be traced almost continuously along the entire orogen (Burg et al., 1984; Burchfiel et al., 1992). Recent estimates of top-NE dip-slip motion on the STDS range from 190 km in western Nepal (Borja et al., 2013) to 100–200 km in eastern Nepal (Searle et al., 2003, 2006; Law et al., 2011). Within the Kali Gandaki valley, field structural observations from the STDS indicate late-stage, top-SW (reverse) shortening that deforms earlier top-NE (normal) shear-related fabrics and leucogranites (Fig. 8). These structures are localized and probably reflect only minor amounts of shortening. Microstructures also indicate a top-SW shear sense in some samples from the STDS (Fig. 9). This late-stage shortening has been reported by other authors (Brown and Nazarchuk, 1993; Hodges et al., 1996; Godin et al., 1999a; Godin, 2003; Larson and Godin, 2009; Parsons et al., 2016) and correlated with D4 deformation in the THS, and with syn- to postpeak metamorphism in the UGHS along the KSZ in the Kali Gandaki valley (Vannay and Hodges, 1996; Godin et al., 1999a; Godin, 2003) and the MKSZ in the Modi Khola valley (Hodges et al., 1996).

Many authors favor the explanation that the STDS is a fixed hanging-wall stretching fault and/or shear zone (*sensu* Means, 1989) that formed in response to the rheological contrast between the hot, weak southward-flowing UGHS (footwall) and the cold, strong stationary THS (hanging wall) (Searle et al., 2003; Williams et al., 2006; Searle, 2010; Law et al., 2011; Kellett and Grujic, 2012). Such a situation reflects the development of a superstructure (i.e., THS)–infrastructure (i.e., UGHS) association (e.g., Williams et al., 2006; Jamieson and Beaumont, 2013) and implies that the STDS is inherently linked to the rheology of the Himalayan orogen. This is the only explanation for formation of the STDS that has been replicated by thermomechanical models of Himalayan orogenesis (Beaumont et al., 2001, 2004). Other tectonic models for the Himalayan orogeny have failed to produce a mechanically working explanation for for-

mation of the STDS (e.g., Jamieson and Beaumont, 2013). This point is echoed by thermomechanical channel-flow models simulated without a significant rheology contrast between mid- and upper-crustal levels, which were unable to produce an STDS-equivalent structure (Model 3, Beaumont et al., 2004). These findings imply that the STDS formed in response to the rheological weakening of the Himalayan-Tibetan mid-crust (UGHS), which caused the upper (THS) and middle (UGHS) crust to mechanically decouple, allowing southward return flow of the UGHS and northward underthrusting of the Indian lower crust, relative to the overlying stationary THS (e.g., Kellett and Grujic, 2012). Subsequently, above a threshold viscosity, rheological strengthening of the UGHS led to the cessation of channel-flow and mechanical recoupling of crustal units. Thus it follows that late-stage top-SW shortening in the STDS may correspond to northward underthrusting of the Indian lower crust, following the cessation of channel-flow and mechanical recoupling of the THS and GHS.

Godin et al. (2001) postulate that an $^{40}\text{Ar}/^{39}\text{Ar}$ muscovite age of ca. 18 Ma from the lowermost THS records the growth and crystallization of muscovite during D4 deformation. Within the UGHS and STDS, D4 deformation structures (Figs. 6 and 8) indicate that the UGHS was still hot and weak enough to deform via pervasive ductile shearing during this deformation phase. As such, the timing of top-SW shortening associated with D4 deformation in the STDS, UGHS, and THS is bracketed between the latest age of D3 top-N shearing on the STDS (22–18.5 Ma; Hodges et al., 1996; Godin et al., 2001) and wholesale exhumation of the UGHS above the muscovite closure temperature for Ar loss (16–13 Ma; Godin et al., 2001; Vannay and Grasemann, 2001; Martin et al., 2015). This is contemporaneous with retrograde metamorphic conditions of 650–670 °C and 7–8 kbar within Unit I at 25–18 Ma (Iaccarino et al., 2015).

Here we suggest that top-SW shortening in the STDS and associated D4 deformation in the UGHS and THS occurred in response to an increase in viscosity of the UGHS due to cooling during exhumation and its subsequent transformation from an “active channel” (weak) to a “channel plug” (strong) (also referred to as a paleochannel; Beaumont et al., 2004; Godin et al., 2006a; Grujic, 2006). Continued northward underthrusting of the Indian lower crust after this viscosity increase resulted in minor amounts of shortening between the THS and GHS. This was synchronous with top-SW shearing on the KSZ and MKSZ sometime after 22–18.5 Ma and before 16–13 Ma, possibly at 18 Ma (Hodges et al., 1996; Godin et al., 2001; Vannay and Grasemann, 2001; Martin et al., 2015). This scenario is comparable to the regional-scale buckling of the THS and GHS reported from the Manaslu Himalaya in central Nepal (Fig. 1B) that occurred in response to the “locking-up” (i.e., cessation) of mid-crustal flow of the GHS and subsequent recoupling of the GHS and THS during continued top-S convergence (Godin et al., 2006b).

4.4. Metamorphic Discontinuities in the Context of Channel Flow

In the Modi Khola valley, metamorphic discontinuities at the base of the UGHS have been interpreted by some authors as faults (the Sinuwa and Bhanuwa faults) between discrete thrust slices (Martin et al., 2010; Corrie and

Kohn, 2011). Claims that these discontinuities refute the occurrence of channel flow (Martin et al., 2010; Corrie and Kohn, 2011) can be reconciled if faulting occurred after the cessation of mid-crustal flow (e.g., Cottle et al., 2015). However, there are no field- or micro-structural observations to support the interpretation of these metamorphic discontinuities as faults. Nor is there evidence for significant annealing and static recrystallization that might have overprinted and obscured such structures.

Alternatively, metamorphic discontinuities can be explained by consideration of the relative velocity profile of a channel flow (Mancktelow, 1995; Grujic, 2006). Southward-directed channel flow during the Himalayan orogeny requires a viscosity reduction at mid-crustal levels, so that the overburden-induced, southward lateral pressure gradient (Poiseuille flow) can overcome the northward crustal flow produced by drag of the lower Indian crust (Couette flow) (Mancktelow, 1995; Turcotte and Schubert, 2002; Grujic, 2006). The resulting velocity profile resembles that of a “hybrid flow” (Grujic, 2006) composed of an upper portion of southward-exhuming, pressure-gradient-driven “return flow” and a lower portion of northward-burying flow (Fig. 12) (Mancktelow, 1995; Grujic, 2006). Within the northward-burying flow, the magnitude of northward velocity increases toward the base of the UGHS. Consequently, across a vertical transect through the channel, particles at the base of the northward-burying section have younger ages of prograde metamorphism and partial melting than particles at the top of the northward-burying section (Fig. 12). Pressure-temperature-time discontinuities could also develop if flow within the channel was discontinuous, due to localized variations in viscosity that would not necessarily be identifiable in the field. On this basis, combined with the absence of field structural evidence to support the presence of the inferred Sinuwa and Bhanuwa faults, it is argued that the aforementioned metamorphic discontinuities at the base of the UGHS in the Annapurna-Dhaulagiri Himalaya do not represent discrete faults and thrust slices. The proposed metamorphic discontinuities can be produced during pervasive ductile deformation (e.g., Mottram et al., 2014) and are entirely compatible with the channel-flow model.

■ 5. IMPLICATIONS FOR THE CHANNEL-FLOW MODEL IN THE ANNAPURNA-DHAULAGIRI HIMALAYA

Geochronometric and thermobarometric constraints presented in this study and others indicate that the UGHS in this region underwent a prolonged phase of partial melting and kyanite-grade metamorphism between 41 and 18.5 Ma (Nazarchuk, 1993; Kaneko, 1995; Hodges et al., 1996; Godin et al., 2001; Martin et al., 2010; Corrie and Kohn, 2011; Kohn and Corrie, 2011; Carosi et al., 2015; Iaccarino et al., 2015; Larson and Cottle, 2015). During this time, coeval top-SW and top-NE motion occurred on the CT and AD/DD, respectively (Nazarchuk, 1993; Hodges et al., 1996; Godin et al., 2001). Both coaxial and non-coaxial, synmigmatitic, transpositional deformations (early fabrics transposed into S3 fabrics) are observed across the UGHS. The trans-

positional nature of D3 deformation between the STDS and THS indicates that the STDS formed as a stretching fault (Means, 1989) and replicates the detachment zone within the superstructure-infrastructure association (e.g., Williams et al., 2006; Jamieson and Beaumont, 2013). The apparent rheological contrast between upper and middle crustal units is likely to be responsible for formation of the STDS between the hot, partially molten, horizontally stretched UGHS (infrastructure) and cold, low-grade, horizontally shortened THS (superstructure) (Williams et al., 2006; Kellett and Godin, 2009; Searle, 2010; Kellett and Grujic, 2012).

Based on the features outlined above, the channel-flow model provides a favorable explanation for mid-crustal evolution of the UGHS in the Annapurna-Dhaulagiri Himalaya, despite its lower-than-typical structural thickness and leucogranite content. However, our findings indicate that the UGHS in the Annapurna-Dhaulagiri Himalaya was more viscous than elsewhere in the Himalaya. Consequently, channel flow in this region was likely to have been more limited (i.e., slower), perhaps with a shorter duration of activity than in other parts of the Himalaya with greater UGHS structural thicknesses and larger melt volumes.

The pervasive and transpositional nature of ductile deformation within the UGHS, which indicates horizontal stretching and vertical shortening, is not compatible with models of thrust stacking and duplex development, which require localization of deformation on discrete thrust planes between competent thrust slices (e.g., Robinson et al., 2006). Likewise, coeval reverse- and normal-sense motion below and above the UGHS, respectively, is yet to be explained with a mechanically working model of any process other than channel flow (e.g., Jamieson and Beaumont, 2013). However, in limiting the rate and/or duration of channel flow, we question whether tectonic processes in the UGHS may reflect a combination of both channel flow and discrete thrusting, particularly when the rheological contrast between different lithologies with different volumes of leucogranite and migmatite is considered. We postulate that in such a situation, pervasive deformation characteristic of channel flow could occur across the whole UGHS, but at different rates in different lithologies. The contacts between different lithologies would represent rheological discontinuities, and in such a situation, it is envisaged that discrete shear zones could form at these boundaries either during or after channel flow. Constraining the PT evolution of each lithological unit in the UGHS would help further investigation of these concepts (e.g., Cottle et al., 2015). Similar models are presented by Cottle et al. (2015) and Jamieson and Beaumont (2013) who propose that channel-flow processes can evolve into thrust stacking processes due to changes in rheology during extrusion and exhumation.

The shallow-inclined PT exhumation path (Fig. 11) indicates that the UGHS exhumed at a slower rate (non-isothermal) than typically recorded elsewhere in the Himalaya (isothermal) and than predicted by particle paths G1 and G2 from channel-flow model HT1 (Jamieson et al., 2004). Slow exhumation of the UGHS is explained by the viscosity-limited subdued nature of channel flow in the Annapurna-Dhaulagiri Himalaya. Our viscosity calculations demonstrate the control of channel thickness and partial melting on viscosity.

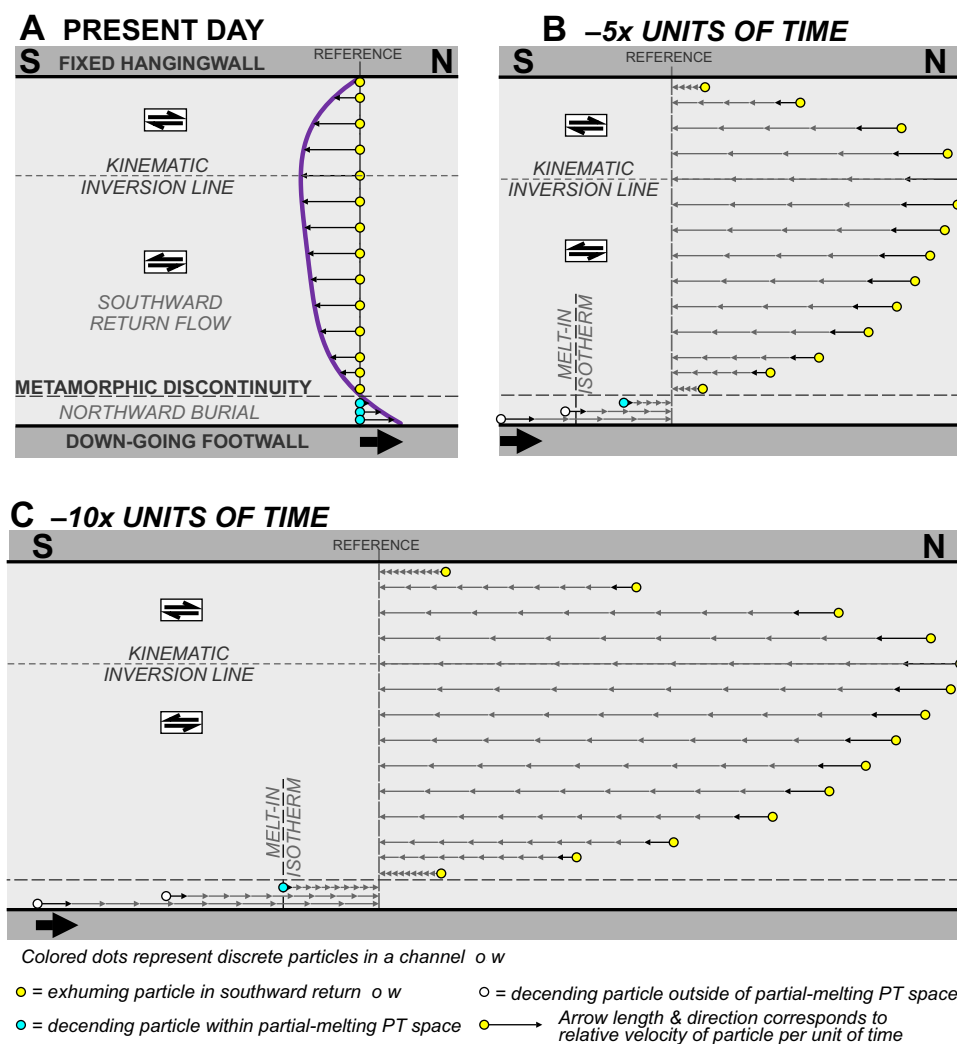


Figure 12. Relative particle motions in a hybrid channel flow. (A) Schematic relative velocity profile (purple line) for a hybrid channel flow with a stress-dependent, power-law rheology (based on equations 6–14 and 7–124, after Turcotte and Schubert, 2002). Upper channel wall is stationary; lower channel wall moves northward (right). Flow is driven by lower channel wall motion and lateral pressure gradient within the channel. Velocity profile drawn relative to stationary upper channel wall. Adjacent particles (colored dots) in an exhumed channel section are derived from different crustal positions due to differences in individual particle pathways. Blue particles have northward-moving burial pathways. Yellow particles have southward-moving exhumation pathways. (B and C) Relative particle positions after –5 and –10 units of time. Variations in relative velocity can result in metamorphic discontinuities between exhuming and burying particles. Within the burial section, timing of initial partial melting decreases down-section from earliest to latest (i.e., youngs down-section).

Importantly, without the production of large amounts of leucogranite (i.e., volume addition), as recorded elsewhere in the Himalaya, vertical shortening during deformation will reduce channel thickness over time and gradually decrease the threshold (i.e., maximum) viscosity at which channel flow can be sustained. Without the greater structural thickness and melt volumes typically recorded elsewhere in the Himalaya, the viscosity of the UGHS in the Annapurna-Dhaulagiri Himalaya was probably too high to facilitate rapid isothermal exhumation. Instead, channel flow gradually “seized up” and ground to a halt

at significant depth (7–8 kbar). This allowed the UGHS to cool, strengthen, and transform from a weak “active channel” to strong “channel plug” at greater depths than in other UGHS-equivalent sections elsewhere in the Himalaya, resulting in slower exhumation.

Correlation between: (1) the timing of retrograde conditions of 650–670 °C and 7–8 kbar at 25–18 Ma and a quartz deformation temperature of 670 ± 50 °C in Unit I; (2) the youngest timing of deformation on the CT and AD/DD at 22–18.5 Ma; and (3) the minimum timing of D4 top-SW shortening in the STDS and

on the KSZ and MKSZ in the UGHS at 18 Ma suggests that this transformation from a weak “active channel” to strong “channel plug” occurred at 22–18 Ma (Nazarchuk, 1993; Hodges et al., 1996; Godin et al., 2001; Larson and Godin, 2009; Iaccarino et al., 2015). We postulate that these conditions correspond to the threshold viscosity for channel flow of the UGHS in the Annapurna-Dhaulagiri Himalaya and record a change in rheology from a pervasively deforming and/or flowing channel (“active channel”) to a coherent block (“channel plug”). Elsewhere along the Himalaya, similar retrograde temperatures recorded in UGHS-equivalent sections were not reached until pressures of 2–6 kbar (Fig. 11). This occurred sometime after 16 Ma in central and eastern Nepal (Searle et al., 2003; Streule et al., 2010; Imayama et al., 2012) and at 14–11 Ma in Bhutan (Daniel et al., 2003; Harris et al., 2004), following exhumation and partial melting well within the sillimanite stability field. Field observations and thermobarometric constraints suggest that following cessation of channel flow in the UGHS, pervasive top-S shearing in the LGHS facilitated the progressive exhumation of the UGHS as a rigid block toward the topographic surface from ~650 °C equivalent depth. This hypothesis is comparable to models proposed by Mottram et al. (2014, 2015) for LGHS-equivalent strata in Bhutan.

6. CONCLUSIONS

Field observations from the Annapurna-Dhaulagiri Himalaya highlight several geological features across the GHS that are distinct from other Himalayan regions. These include low volumes of leucogranite and migmatite, an absence of evidence for partial melting in the sillimanite stability field, a reduced structural thickness, and late-stage top-SW shortening in the STDS. These features are not readily compatible with proposed models for the evolution of the Himalayan orogen, and their implications for the rheological behavior of the GHS in this region must therefore be considered.

Field structural observations, combined with new and previously published thermobarometric and geochronometric constraints indicate that the mid-crustal evolution of the UGHS in the Annapurna-Dhaulagiri Himalaya is more favorably explained by the channel-flow model than models based on thrust-stacking mechanisms. However, consideration of the rheological properties of the UGHS with a specific focus on the effects of melt volume and channel thickness suggests that channel flow was more limited and subdued (i.e., slower) in the Annapurna-Dhaulagiri Himalaya than in other regions where melt volume and structural thickness were larger. Flow-law–derived viscosity estimates of $\sim 10^{20}$ Pa s for the bulk volume of the UGHS also imply that channel flow was slower and more limited than that simulated by thermomechanical channel-flow model HT1 of Beaumont et al. (2004). Furthermore, viscosity calculations demonstrate that without addition of material during channel flow (i.e., leucogranite generation), vertical shortening led to a gradual decrease in the threshold viscosity for flow within the UGHS.

The PTt exhumation path of the UGHS in the Annapurna-Dhaulagiri Himalaya has a shallower gradient (i.e., slower) than in other parts of the Himalaya

where UGHS-equivalent sequences exhumed along isothermal to near-isothermal (i.e., rapid) trajectories. Additionally, the UGHS PTt exhumation path from the Annapurna-Dhaulagiri Himalaya is much shallower than modeled isothermal PTt paths determined from channel-flow model HT1. Our findings suggest that in the Annapurna-Dhaulagiri Himalaya, viscosity-limited, subdued channel flow of the UGHS was not weak enough to facilitate rapid, isothermal exhumation due to its lower-than-average structural thickness and melt volumes. Slower exhumation along a more shallow-inclined PTt path prevented extensive fluid-absent decompression melting within the sillimanite stability field, which compounded the rheological effects of low melt volumes during exhumation even further. Consequently, vertical shortening of ~25%–50% without the addition of large melt volumes led to a gradual deceleration of channel flow as the threshold viscosity for flow decreased. Eventually, the effective viscosity of the UGHS exceeded the threshold viscosity for flow, at which point mid-crustal channel flow could no longer be sustained.

The initiation of D4 deformation associated with top-SW shortening in the STDS and top-SW motion along the KSZ and MKSZ at ca. 18 Ma is believed to reflect the transformation of the UGHS from a weak “active channel” to a strong “channel plug.” Pressure-temperature-time constraints suggest that in the Annapurna-Dhaulagiri Himalaya this transformation, and thus the threshold viscosity for channel flow, occurred at 650–670 °C and 7–8 kbar. Consequently, the UGHS in this region exhumed slowly, cooling and strengthening 2–7 m.y. earlier and at 1–6 kbar greater pressure (~3–18 km deeper) than elsewhere in the central and eastern Himalaya.

These findings are distinct from other regions in the Himalaya, and, as such, we consider the mid-crustal evolution of the GHS in the Annapurna-Dhaulagiri Himalaya to be an *atypical* example of channel flow during the Himalayan orogeny.

ACKNOWLEDGMENTS

We thank Ron Frost, Dawn Kellett, and Claire Warren for their extensive reviews that greatly improved this work, and we also thank Geosphere editors Mike Cheadle and Ray Russo, who oversaw the review and revision process. Mark Caddick and Matt Kohn are thanked for helpful advice concerning the thermobarometry presented in this manuscript. Suka Ghale, Basan Sherpa, and their Nepalese colleagues are thanked for guidance and assistance during fieldwork. The research reported in this paper was supported by Natural Environment Research Council (training grant NE/J50001X/1) to AJP and National Science Foundation grant EAR0711207 to RDL. We thank Research Councils UK for funding the open access publication of this manuscript.

REFERENCES CITED

- Adhikari, B.R., and Wagreich, M., 2011, Provenance evolution of collapse graben fill in the Himalaya—The Miocene to Quaternary Thakkhola-Mustang Graben (Nepal): Sedimentary Geology, v. 233, p. 1–14, doi:10.1016/j.sedgeo.2010.09.021.
- Arita, K., 1983, Origin of the inverted metamorphism of the Lower Himalayas, Central Nepal: Tectonophysics, v. 95, p. 43–60, doi:10.1016/0040-1951(83)90258-5.
- Avouac, J.P., 2015, Mountain building: From earthquakes to geologic deformation, in Schubert, G., ed., Treatise on Geophysics, Second Edition, Volume 6: Oxford, UK, Elsevier, p. 381–432, doi:10.1016/B978-0-444-53802-4.00120-2.
- Baltz, T., 2012, Structural Evolution of Thakkhola Graben: Implications for the Architecture of the Central Himalaya, Nepal [M.S. thesis]: Department of Earth and Atmospheric Sciences, University of Houston, 98 p.

- Beaumont, C., Jamieson, R.A., Nguyen, M.H., and Lee, B., 2001, Himalayan tectonics explained by extrusion of a low-viscosity crustal channel coupled to focused surface denudation: *Nature*, v. 414, p. 738–742, doi:10.1038/414738a.
- Beaumont, C., Jamieson, R.A., Nguyen, M.H., and Medvedev, S., 2004, Crustal channel flows: 1. Numerical models with applications to the tectonics of the Himalayan-Tibetan orogen: *Journal of Geophysical Research. Solid Earth*, v. 109, p. B06406, doi:10.1029/2003JB002809.
- Berman, R.G., 1991, Thermobarometry using multi-equilibrium calculations: A new technique, with petrological applications: *Canadian Mineralogist*, v. 29, p. 833–855.
- Berman, R.G., 2007, Win TWQ (version 2.3): A software package for performing internally-consistent thermobarometric calculations: Geological Survey of Canada Open-File 5462, p. 1–41.
- Berman, R.G., and Aranovich, L.Y., 1996, Optimized standard state and solution properties of minerals: *Contributions to Mineralogy and Petrology*, v. 126, p. 1–24, doi:10.1007/s004100050232.
- Berthé, D., Choukroune, P., and Jegouzo, P., 1979, Orthogneiss, mylonite and non coaxial deformation of granites: The example of the South Armorican Shear Zone: *Journal of Structural Geology*, v. 1, p. 31–42, doi:10.1016/0191-8141(79)90019-1.
- Beyssac, O., Bollinger, L., Avouac, J.P., and Goffe, B., 2004, Thermal metamorphism in the Lesser Himalaya of Nepal determined from Raman spectroscopy of carbonaceous material: *Earth and Planetary Science Letters*, v. 225, p. 233–241, doi:10.1016/j.epsl.2004.05.023.
- Bollinger, L., Avouac, J.P., Beyssac, O., Catlos, E.J., Harrison, T.M., Grove, M., Goffe, B., and Sapkota, S., 2004, Thermal structure and exhumation history of the Lesser Himalaya in central Nepal: *Tectonics*, v. 23, doi:10.1029/2003TC001564.
- Bollinger, L., Henry, P., and Avouac, J.P., 2006, Mountain building in the Nepal Himalaya: Thermal and kinematic model: *Earth and Planetary Science Letters*, v. 244, p. 58–71, doi:10.1016/j.epsl.2006.01.045.
- Borja, A., Godin, L., Wemmer, K., and Nagy, C., 2013, Kinematics of the Dadeldhura klippe shear zones (W Nepal): Implications for the foreland evolution of the Himalayan metamorphic core: *Terra Nova*, v. 25, p. 282–291, doi:10.1111/ter.12034.
- Bouchez, J.-L., and Pêcher, A., 1981, The Himalayan Main Central Thrust pile and its quartz-rich tectonites in central Nepal: *Tectonophysics*, v. 78, p. 23–50, doi:10.1016/0040-1951(81)90004-4.
- Brown, R.L., and Nazarchuk, J.H., 1993, Annapurna detachment fault in the Greater Himalaya of Central Nepal, in Treloar, P.J., and Searle, M.P., eds., *Himalayan Tectonics: Geological Society of London Special Publications* 74, p. 461–473, doi:10.1144/GSL.SP.1993.074.01.31.
- Burchfiel, B.C., Zhiliang, C., Hodges, K.V., Yüping, L., Royden, L.H., Changrong, D., and Jiene, X., 1992, The South Tibetan Detachment System, Himalaya Orogen: Extension Contemporaneous With and Parallel to Shortening in a Collisional Mountain Belt: *Geological Society of America Special Paper* 269, p. 1–41, doi:10.1130/SPE269-p1.
- Burg, J.P., Brunel, M., Gapais, D., Chen, G.M., and Liu, G.H., 1984, Deformation of leucogranites of the crystalline Main Central Sheet in southern Tibet (China): *Journal of Structural Geology*, v. 6, p. 535–542, doi:10.1016/0191-8141(84)90063-4.
- Caddick, M.J., 2005, *Tectono-metamorphic Evolution of the central and western Himalaya* [Ph.D. thesis]: University of Cambridge.
- Caddick, M.J., Bickle, M.J., Harris, N.B.W., Holland, T.J.B., Horstwood, M.S.A., Parrish, R.R., and Ahmad, T., 2007, Burial and exhumation history of a Lesser Himalayan schist: Recording the formation of an inverted metamorphic sequence in NW India: *Earth and Planetary Science Letters*, v. 264, p. 375–390, doi:10.1016/j.epsl.2007.09.011.
- Caristan, Y., 1982, The transition from high temperature creep to fracture in Maryland diabase: *Journal of Geophysical Research*, v. 87, B8, p. 6781–6790, doi:10.1029/JB087iB08p06781.
- Carosi, R., Montomali, C., Langone, A., Turina, A., Cesare, B., Iaccarino, S., Fascioli, L., Visonà, D., Ronchi, A., and Rai, S.M., 2015, Eocene partial melting recorded in peritectic garnets from kyanite-gneiss, Greater Himalayan Sequence, central Nepal, in Mukherjee, S., Carosi, R., Van Der Beek, P.K., Mukherjee, B.K., and Robinson, D.M., eds., *Tectonics of the Himalaya: Geological Society of London Special Publications*, v. 412, p. 111–129. First published online September 9, 2014, doi:10.1144/SP412.1.
- Colchen, M., Le Fort, P., and Pêcher, A., 1981, Geological map of Annapurnas-Manaslu-Ganesh Himalaya of Nepal, in Gupta, H.K., Delany, F.M., eds., *Zagros-Hindu Kush-Himalaya Geodynamic Evolution: Washington, D.C., American Geophysical Union*, scale 1:200,000.
- Corrie, S.L., and Kohn, M.J., 2011, Metamorphic history of the central Himalaya, Annapurna region, Nepal, and implications for tectonic models: *Geological Society of America Bulletin*, v. 123, p. 1863–1879, doi:10.1130/B30376.1.
- Cottle, J.M., Waters, D.J., Riley, D., Beyssac, O., and Jessup, M.J., 2011, Metamorphic history of the South Tibetan Detachment System, Mt. Everest region, revealed by RSCM thermometry and phase equilibria modelling: *Journal of Metamorphic Geology*, v. 29, p. 561–582, doi:10.1111/j.1525-1314.2011.00930.x.
- Cottle, J.M., Larson, K.P., and Kellett, D.A., 2015, How does the mid-crust accommodate deformation in large, hot collisional orogens?: A review of recent research in the Himalayan orogen: *Journal of Structural Geology*, v. 78, p. 119–133, doi:10.1016/j.jsg.2015.06.008.
- Daniel, C.G., Hollister, L.S., Parrish, R.R., and Grujic, D., 2003, Exhumation of the Main Central Thrust from lower crustal depths, eastern Bhutan Himalaya: *Journal of Metamorphic Geology*, v. 21, p. 317–334, doi:10.1046/j.1525-1314.2003.00445.x.
- Dasgupta, S., Ganguly, J., and Neogi, S., 2004, Inverted metamorphic sequence in the Sikkim Himalayas: Crystallization history, P-T gradient and implications: *Journal of Metamorphic Geology*, v. 22, p. 395–412, doi:10.1111/j.1525-1314.2004.00522.x.
- Dhital, M.R., 2015, *Geology of the Nepal Himalaya: Regional Perspective of the Classic Collided Orogen*: New York, Springer, 498 p., doi:10.1007/978-3-319-02496-7.
- Frassi, C., 2015, Dominant simple-shear deformation during peak metamorphism for the lower portion of the Greater Himalayan Sequence in West Nepal: New implications for hybrid channel flow-type mechanisms in the Dolpo region: *Journal of Structural Geology*, v. 81, p. 28–44, doi:10.1016/j.jsg.2015.10.002.
- Frost, B.R., and Chacko, T., 1989, The granulite uncertainty principle: Limitations on thermobarometry in granulites: *The Journal of Geology*, v. 97, p. 435–450, doi:10.1086/629321.
- Garzanti, E., 1999, Stratigraphy and sedimentary history of the Nepal Tethys Himalaya passive margin: *Journal of Asian Earth Sciences*, v. 17, p. 805–827, doi:10.1016/S1367-9120(99)00017-6.
- Garzzone, C.N., Decelles, P.G., Hodkinson, D.G., Ojha, T.P., and Upreti, B.N., 2003, East-west extension and Miocene environmental change in the southern Tibetan plateau: Thakkhola graben, central Nepal: *Geological Society of America Bulletin*, v. 115, p. 3–20, doi:10.1130/0016-7606(2003)115<0003:EWEAME>2.0.CO;2.
- Gleason, G.C., and Tullis, J., 1995, A flow law for dislocation creep of quartz aggregates determined with the molten-salt cell: *Tectonophysics*, v. 247, p. 1–23, doi:10.1016/0040-1951(95)00011-B.
- Gleeson, T.P., and Godin, L., 2006, The Chako antiform: A folded segment of the Greater Himalayan sequence, Nar Valley, Central Nepal Himalaya: *Journal of Asian Earth Sciences*, v. 27, p. 717–734, doi:10.1016/j.jseae.2005.06.011.
- Godin, L., 2003, Structural evolution of the Tethyan sedimentary sequence in the Annapurna area, central Nepal Himalaya: *Journal of Asian Earth Sciences*, v. 22, p. 307–328, doi:10.1016/S1367-9120(03)00066-X.
- Godin, L., Brown, R.L., and Hanmer, S., 1999a, High strain zone in the hanging wall of the Annapurna detachment, central Nepal Himalaya, in Macfarlane, A., Sorkhabi, R.B., and Quade, J., eds., *Himalaya and Tibet: Mountain Roots to Mountain Tops: Geological Society of America Special Paper* 328, p. 199–210, doi:10.1130/0-8137-2328-0.199.
- Godin, L., Brown, R.L., Hanmer, S., and Parrish, R., 1999b, Back folds in the core of the Himalayan orogen: An alternative interpretation: *Geology*, v. 27, p. 151–154, doi:10.1130/0091-7613(1999)027<0151:BFITCO>2.3.CO;2.
- Godin, L., Parrish, R.R., Brown, R.L., and Hodges, K.V., 2001, Crustal thickening leading to exhumation of the Himalayan metamorphic core of central Nepal: Insight from U-Pb geochronology and ⁴⁰Ar/³⁹Ar thermochronology: *Tectonics*, v. 20, p. 729–747, doi:10.1029/2000TC001204.
- Godin, L., Grujic, D., Law, R.D., and Searle, M.P., 2006a, Channel flow, ductile extrusion and exhumation in continental collision zones: An introduction, in Law, R.D., Searle, M.P., and Godin, L., eds., *Channel Flow, Ductile Extrusion and Exhumation in Continental Collision Zones: Geological Society of London Special Publications*, v. 268, p. 1–23, doi:10.1144/GSL.SP.2006.268.01.01.
- Godin, L., Gleeson, T.P., Searle, M.P., Ullrich, T.D., and Parrish, R.R., 2006b, Locking of southward extrusion in favour of rapid crustal-scale buckling of the Greater Himalayan sequence, Nar valley, central Nepal, in Law, R.D., Searle, M.P., and Godin, L., eds., *Channel Flow, Ductile Extrusion and Exhumation in Continental Collision Zones: Geological Society of London Special Publications*, v. 268, p. 269–292, doi:10.1144/GSL.SP.2006.268.01.13.
- Goscombe, B., Gray, D., and Hand, M., 2006, Crustal architecture of the Himalayan metamorphic front in eastern Nepal: *Gondwana Research*, v. 10, p. 232–255, doi:10.1016/j.gr.2006.05.003.
- Gradstein, F.M., Von Rad, U., Gibling, M.R., Jansa, L.F., Kaminski, M.A., Kristiansen, I.L., Ogg, J.G., Roehl, U., Sarti, M., Thürow, J.W., Westermann, G.E.G., and Wiedmann, J., 1992, Stratigraphy and depositional history of the Mesozoic continental margin of central Nepal: *Geologisches Jahrbuch. Reihe B, Regionale Geologie Ausland*, v. 77, p. 1–141.
- Grasemann, B., Fritz, H., and Vannay, J.C., 1999, Quantitative kinematic flow analysis from the Main Central Thrust Zone (NW-Himalaya, India): Implications for a decelerating strain path

- and the extrusion of orogenic wedges: *Journal of Structural Geology*, v. 21, p. 837–853, doi:10.1016/S0191-8141(99)00077-2.
- Grasemann, B., Edwards, M.A., and Wiesmayr, G., 2006, Kinematic dilatancy effects on orogenic extrusion, *in* Law, R.D., Searle, M.P., and Godin, L., eds., *Channel Flow, Ductile Extrusion and Exhumation in Continental Collision Zones*: Geological Society of London Special Publications, v. 268, p. 25–37, doi:10.1144/Gsl.Sp.2006.268.01.08.
- Green, O.R., Searle, M.P., Corfield, R.I., and Corfield, R.M., 2008, Cretaceous–Tertiary carbonate platform evolution and the age of the India–Asia collision along the Ladakh Himalaya (North-west India): *The Journal of Geology*, v. 116, p. 331–353, doi:10.1086/588831.
- Grujic, D., 2006, Channel flow and continental collision tectonics: An overview, *in* Law, R.D., Searle, M.P., and Godin, L., eds., *Channel Flow, Ductile Extrusion and Exhumation in Continental Collision Zones*: Geological Society of London Special Publications, v. 268, p. 25–37, doi:10.1144/GSL.SP.2006.268.01.02.
- Grujic, D., Casey, M., Davidson, C., Hollister, L.S., Kundig, R., Pavlis, T., and Schmid, S., 1996, Ductile extrusion of the Higher Himalayan Crystalline in Bhutan: Evidence from quartz microfabrics: *Tectonophysics*, v. 260, p. 21–43, doi:10.1016/0040-1951(96)00074-1.
- Grujic, D., Hollister, L.S., and Parrish, R.R., 2002, Himalayan metamorphic sequence as an orogenic channel: Insight from Bhutan: *Earth and Planetary Science Letters*, v. 198, p. 177–191, doi:10.1016/S0012-821X(02)00482-X.
- Guillot, S., Cosca, M., Allemand, P., and Le Fort, P.L., 1999, Contrasting metamorphic and geochronological evolution along the Himalayan belt, *in* Macfarlane, A., Sorkhabi, R.B., and Quade, J., eds., *Himalaya and Tibet: Mountain Roots to Mountain Tops*: Geological Society of America Special Paper 328, p. 117–128, doi:10.1130/0-8137-2328-0.117.
- Handy, M.R., 1990, The solid-state flow of polycrystalline rocks: *Journal of Geophysical Research*, Solid Earth, v. 95, p. 8647–8661, doi:10.1029/JB095iB06p08647.
- Hansen, F., and Carter, N., 1983, Semibrittle Creep of Dry and Wet Westerly Granite at 1000 MPa: College Station, Texas, The 24th U.S. Symposium on Rock Mechanics (USRMS), American Rock Mechanics Association.
- Harris, N., 2007, Channel flow and the Himalayan–Tibetan orogen: A critical review: *Journal of the Geological Society*, v. 164, p. 511–523, doi:10.1144/0016-76492006-133.
- Harris, N., and Massey, J., 1994, Decompression and anatexis of Himalayan metapelites: *Tectonics*, v. 13, p. 1537–1546, doi:10.1029/94TC01611.
- Harris, N.B.W., Caddick, M., Kosler, J., Goswami, S., Vance, D., and Tindle, A.G., 2004, The pressure–temperature–time path of migmatites from the Sikkim Himalaya: *Journal of Metamorphic Geology*, v. 22, p. 249–264, doi:10.1111/j.1525-1314.2004.00511.x.
- Harrison, T.M., Grove, M., McKeegan, K.D., Coath, C.D., Lovera, O.M., and Le Fort, P., 1999, Origin and episodic emplacement of the Manaslu intrusive complex, central Himalaya: *Journal of Petrology*, v. 40, p. 3–19, doi:10.1093/ptro/40.1.3.
- Hayden, L., Watson, E.B., and Wark, D., 2008, A thermobarometer for sphene (titanite): *Contributions to Mineralogy and Petrology*, v. 155, p. 529–540, doi:10.1007/s00410-007-0256-y.
- He, D., Webb, A.G., Larson, K.P., Martin, A.J., and Schmitt, A.K., 2014, Extrusion vs. duplexing models of Himalayan mountain building 3: Duplexing dominates from the Oligocene to Present: *International Geology Review*, v. 57, p. 1–27, doi:10.1080/00206814.2014.986669.
- Hodges, K.V., and McKenna, L.W., 1987, Realistic propagation of uncertainties in geologic thermobarometry: *The American Mineralogist*, v. 72, p. 671–680.
- Hodges, K.V., Burchfiel, B.C., Royden, L.H., Chen, Z., and Liu, Y., 1993, The metamorphic signature of contemporaneous extension and shortening in the central Himalayan orogen: Data from the Nyalam transect, southern Tibet: *Journal of Metamorphic Geology*, v. 11, p. 721–737, doi:10.1111/j.1525-1314.1993.tb00183.x.
- Hodges, K.V., Parrish, R.R., and Searle, M.P., 1996, Tectonic evolution of the central Annapurna Range, Nepalese Himalayas: *Tectonics*, v. 15, p. 1264–1291, doi:10.1029/96TC01791.
- Hurtado, J.M., Hodges, K.V., and Whipple, K.X., 2001, Neotectonics of the Thakkhola graben and implications for recent activity on the South Tibetan fault system in the central Nepal Himalaya: *Geological Society of America Bulletin*, v. 113, p. 222–240, doi:10.1130/0016-7606(2001)113<0222:NOTTGA>2.0.CO;2.
- Iaccarino, S., Montomoli, C., Carosi, R., Massonne, H.-J., Langone, A., and Visonà, D., 2015, Pressure–temperature–time–deformation path of kyanite-bearing migmatitic paragneiss in the Kali Gandaki valley (Central Nepal): Investigation of Late Eocene–Early Oligocene melting processes: *Lithos*, v. 231, p. 103–121, doi:10.1016/j.lithos.2015.06.005.
- Imayama, T., Takeshite, T., Yi, K., Cho, D.-L., Kitajima, K., Tsutsumi, Y., Kayama, M., Nishido, H., Okumura, T., Yagi, K., Itaya, T., and Sano, Y., 2012, Two-stage partial melting and contrasting cooling history within the Higher Himalayan Crystalline Sequence in the far-eastern Nepal Himalaya: *Lithos*, v. 134–135, p. 1–22, doi:10.1016/j.lithos.2011.12.004.
- Inger, S., and Harris, N.B.W., 1992, Tectonothermal Evolution of the High Himalayan Crystalline Sequence, Langtang Valley, Northern Nepal: *Journal of Metamorphic Geology*, v. 10, p. 439–452, doi:10.1111/j.1525-1314.1992.tb00095.x.
- Jamieson, R.A., and Beaumont, C., 2013, On the origin of orogens: *Geological Society of America Bulletin*, v. 125, p. 1671–1702, doi:10.1130/b30855.1.
- Jamieson, R.A., Beaumont, C., Medvedev, S., and Nguyen, M.H., 2004, Crustal channel flows: 2. Numerical models with implications for metamorphism in the Himalayan–Tibetan orogen: *Journal of Geophysical Research*, Solid Earth, v. 109, p. B06407, doi:10.1029/2003jb002811.
- Jamieson, R.A., Beaumont, C., Nguyen, M.H., and Grujic, D., 2006, Provenance of the Greater Himalayan Sequence and associated rocks: predictions of channel-flow models, *in* Law, R.D., Searle, M.P., and Godin, L., eds., *Channel Flow, Ductile Extrusion and Exhumation in Continental Collision Zones*: Geological Society of London Special Publications, v. 268, p. 165–182, doi:10.1144/GSL.SP.2006.268.01.07.
- Jamieson, R.A., Unsworth, M.J., Harris, N.B.W., Rosenberg, C.L., and Schulmann, K., 2011, Crustal melting and the flow of mountains: *Mineralogical Society of America, Elements*, v. 7, p. 253–260, doi:10.2113/gselements.74.253.
- Jaoul, O., Tullis, J., and Kronenberg, A., 1984, The effect of varying water contents on the creep behavior of Heavtree quartzite: *Journal of Geophysical Research*, v. 89, B6, p. 4298–4312, doi:10.1029/JB089iB06p04298.
- Jessup, M.J., Law, R.D., Searle, M.P., and Hubbard, M.S., 2006, Structural evolution and vorticity of flow during extrusion and exhumation of the Greater Himalayan Slab, Mount Everest Massif, Tibet/Nepal: Implications for orogen-scale flow partitioning, *in* Law, R.D., Searle, M.P., and Godin, L., eds., *Channel Flow, Ductile Extrusion and Exhumation in Continental Collision Zones*: Geological Society of London Special Publications 268, p. 379–413, doi:10.1144/GSL.SP.2006.268.01.18.
- Kaneko, Y., 1995, Thermal structure in the Annapurna region, central Nepal Himalaya: implication for the inverted metamorphism: *Journal of Mineralogy, Petrology and Economic Geology*, v. 90, p. 143–154, doi:10.2465/ganko.90.143.
- Kellett, D.A., and Godin, L., 2009, Pre-Miocene deformation of the Himalayan superstructure, Hidden valley, central Nepal: *Journal of the Geological Society*, v. 166, p. 261–275, doi:10.1144/0016-76492008-097.
- Kellett, D.A., and Grujic, D., 2012, New insight into the South Tibetan detachment system: Not a single progressive deformation: *Tectonics*, v. 31, p. TC2007, doi:10.1029/2011TC002957.
- Kohn, M.J., 2008, P–T–t data from central Nepal support critical taper and repudiate large-scale channel flow of the Greater Himalayan Sequence: *Geological Society of America Bulletin*, v. 120, p. 259–273, doi:10.1130/B26252.1.
- Kohn, M.J., 2014, Himalayan metamorphism and its tectonic implications: *Annual Review of Earth and Planetary Sciences*, v. 42, p. 381–419, doi:10.1146/annurev-earth-060313-055005.
- Kohn, M.J., and Corrie, S.L., 2011, Preserved Zr-temperatures and U–Pb ages in high-grade metamorphic titanite: Evidence for a static hot channel in the Himalayan orogen: *Earth and Planetary Science Letters*, v. 311, p. 136–143, doi:10.1016/j.epsl.2011.09.008.
- Kohn, M.J., and Spear, F., 2000, Retrograde net transfer reaction insurance for pressure–temperature estimates: *Geology*, v. 28, p. 1127–1130, doi:10.1130/0091-7613(2000)28<1127:RNTRIF>2.0.CO;2.
- Kohn, M.J., Orange, D.L., Spear, F.S., Rumble, D., and Harrison, T.M., 1992, Pressure, temperature, and structural evolution of West-Central New Hampshire: Hot thrusts over cold basement: *Journal of Petrology*, v. 33, p. 521–556, doi:10.1093/ptrology/33.3.521.
- Kronenberg, A.K., Hasnan, H.F.B., Holyoke, C.W., III, Kronenberg, J.A., Law, R.D., and Thomas, J.B., 2014, FTIR maps and spatial distributions of OH in Caledonide and Himalayan shear zones: Implications for dislocation creep and water weakening: *San Francisco, California, American Geophysical Union Annual Meeting, abstract T13A-4619*.
- Kruhl, J.H., 1998, Reply: Prism- and basal-plane parallel subgrain boundaries in quartz: A microstructural geothermobarometer: *Journal of Metamorphic Geology*, v. 16, p. 142–146, doi:10.1111/j.1525-1314.1998.00063.x.
- Larson, K.P., and Cottle, J.M., 2015, Initiation of crustal shortening in the Himalaya: *Terra Nova*, v. 27, p. 169–174, doi:10.1111/ter.12145.
- Larson, K.P., and Godin, L., 2009, Kinematics of the Greater Himalayan sequence, Dhaulagiri Himal: Implications for the structural framework of central Nepal: *Journal of the Geological Society*, v. 166, p. 25–43, doi:10.1144/0016-76492007-180.

- Larson, K.P., Godin, L., and Price, R.A., 2010, Relationships between displacement and distortion in orogens: Linking the Himalayan foreland and hinterland in central Nepal: *Geological Society of America Bulletin*, v. 122, p. 1116–1134, doi:10.1130/B30073.1.
- Law, R.D., Jessup, M.J., Searle, M.P., Francis, M.K., Walters, D.J., and Cottle, J.M., 2011, Tele-scopeing of isotherms beneath the South Tibetan Detachment System, Mount Everest Massif: *Journal of Structural Geology*, v. 33, p. 1569–1594, doi:10.1016/j.jsg.2011.09.004.
- Law, R.D., Stahr Iii, D.W., Francis, M.K., Ashley, K.T., Grasemann, B., and Ahmad, T., 2013, Deformation temperatures and flow vorticities near the base of the Greater Himalayan Series, Sutlej Valley and Shimla Klippe, NW India: *Journal of Structural Geology*, v. 54, p. 21–53, doi:10.1016/j.jsg.2013.05.009.
- Le Fort, P., 1975, Himalayas: The collided range. Present knowledge of the continental arc: *American Journal of Science*, v. 275-A, p. 1–44.
- Le Fort, P., Pêcher, A., and Upreti, B.N., 1986, A section through the Tibetan Slab in Central Nepal (Kali Gandaki valley): Mineral chemistry and thermobarometry of the Main Central Thrust zone, in Le Fort, P., Colchen, M., and Montenat, C., eds., *Orogenic Evolution of Southern Asia (from Turkey to Indonesia)*: Nancy, France, Sciences de la Terre, p. 211–228, doi:10.1029/JB086iB11p10545.
- Mancktelow, N.S., 1995, Nonlithostatic pressure during sediment subduction and the development and exhumation of high-pressure metamorphic rocks: *Journal of Geophysical Research. Solid Earth*, v. 100, p. 571–583, doi:10.1029/94JB02158.
- Martin, A.J., Decelles, P.G., Gehrels, G.E., Patchett, P.J., and Isachsen, C., 2005, Isotopic and structural constraints on the location of the Main Central thrust in the Annapurna Range, central Nepal Himalaya: *Geological Society of America Bulletin*, v. 117, p. 926–944, doi:10.1130/B25646.1.
- Martin, A.J., Ganguly, J., and Decelles, P.G., 2010, Metamorphism of Greater and Lesser Himalayan rocks exposed in the Modi Khola valley, central Nepal: *Contributions to Mineralogy and Petrology*, v. 159, p. 203–223, doi:10.1007/s00410-009-0424-3.
- Martin, A.J., Copeland, P., and Benowitz, J.A., 2015, Muscovite $^{40}\text{Ar}/^{39}\text{Ar}$ ages help reveal the Neogene tectonic evolution of the southern Annapurna Range, central Nepal, in Mukherjee, S., Carosi, R., Van Der Beek, P.K., Mukherjee, B.K., and Robinson, D.M., eds., *Tectonics of the Himalaya*: Geological Society of London Special Publications, v. 412, p. 199–220, doi:10.1144/SP412.5.
- Means, W.D., 1989, Stretching Faults: *Geology*, v. 17, p. 893–896, doi:10.1130/0091-7613(1989)017<0893:SF>2.3.CO;2.
- Montomoli, C., Carosi, R., and Iaccarino, S., 2015, Tectonometamorphic discontinuities in the Greater Himalayan Sequence: A local or a regional feature?, in Mukherjee, S., Carosi, R., Van Der Beek, P.K., Mukherjee, B.K., and Robinson, D.M., eds., *Tectonics of the Himalaya*: Geological Society of London Special Publications, v. 412, p. 25–41, doi:10.1144/sp412.3.
- Mottram, C.M., Argles, T.W., Harris, N.B.W., Parrish, R.R., Horstwood, M.S.A., Warren, C.J., and Gupta, S., 2014, Tectonic interleaving along the Main Central Thrust, Sikkim Himalaya: *Journal of the Geological Society*, v. 171, p. 255–268, doi:10.1144/jgs2013-064.
- Mottram, C.M., Parrish, R.R., Regis, D., Warren, C.J., Argles, T.W., Harris, N.B.W., and Roberts, N.M.W., 2015, Using U-Th-Pb petrochronology to determine rates of ductile thrusting: Time windows into the Main Central Thrust, Sikkim Himalaya: *Tectonics*, v. 34, doi:10.1002/2014TC003743.
- Mukherjee, S., 2013a, Channel flow extrusion model to constrain dynamic viscosity and Prandtl number of the Higher Himalayan Shear Zone: *International Journal of Earth Sciences*, v. 102, p. 1811–1835, doi:10.1007/s00531-012-0806-z.
- Mukherjee, S., 2013b, Higher Himalaya in the Bhagirathi section (NW Himalaya, India): Its structures, backthrusts and extrusion mechanism by both channel flow and critical taper mechanisms: *International Journal of Earth Sciences*, v. 102, p. 1851–1870, doi:10.1007/s00531-012-0861-5.
- Najman, Y., Appel, E., Boudagher-Fadel, M., Bown, P., Carter, A., Garzanti, E., Godin, L., Han, J., Liebke, U., Oliver, G., Parrish, R., and Vezzoli, G., 2010, Timing of India-Asia collision: Geological, biostratigraphic, and palaeomagnetic constraints: *Journal of Geophysical Research. Solid Earth*, v. 115, p. B12416, doi:10.1029/2010JB007673.
- Nazarchuk, J.H., 1993, Structure and geochronology of the Greater Himalaya, Kali Gandaki region, west-central Nepal [M.S. thesis]: Ottawa, Ontario, Carleton University.
- Nelson, K.D., Zhao, W.J., Brown, L.D., Kuo, J., Che, J.K., Liu, X.W., Klemperer, S.L., Makovsky, Y., Meissner, R., Mechie, J., Kind, R., Wenzel, F., Ni, J., Nabelek, J., Chen, L.S., Tan, H.D., Wei, W.B., Jones, A.G., Booker, J., Unsworth, M., Kidd, W.S.F., Hauck, M., Alsdorf, D., Ross, A., Cogan, M., Wu, C.D., Sandvol, E., and Edwards, M., 1996, Partially molten middle crust beneath southern Tibet: Synthesis of project INDEPTH results: *Science*, v. 274, p. 1684–1688, doi:10.1126/science.274.5293.1684.
- Parsons, A.J., Law, R.D., Searle, M.P., Phillips, R.J., and Lloyd, G.E., 2016, Geology of the Dhaulagiri-Annapurna-Manaslu Himalaya, Western Region, Nepal. 1:200,000: *Journal of Maps*, v. 12, p. 100–110, doi:10.1080/17445647.2014.984784.
- Passchier, C.W., and Trouw, R.A.J., 2005, *Microtectonics*, Second edition: New York, Springer, 366 p.
- Paudel, L.P., and Arita, K., 2006, Thermal evolution of the Lesser Himalaya, central Nepal: Insights from K-white micas compositional variation: *Gondwana Research*, v. 9, p. 409–425, doi:10.1016/j.gr.2006.01.003.
- Pêcher, A., 1989, The metamorphism in the Central Himalaya: *Journal of Metamorphic Geology*, v. 7, p. 31–41, doi:10.1111/j.1525-1314.1989.tb00573.x.
- Robinson, D.M., Decelles, P.G., and Copeland, P., 2006, Tectonic evolution of the Himalayan thrust belt in western Nepal: Implications for channel-flow models: *Geological Society of America Bulletin*, v. 118, p. 865–885, doi:10.1130/B25911.1.
- Rosenberg, C., Medvedev, S., and Handy, M., 2007, Effects of melting on faulting and continental deformation, in Handy, M.R., Hirth, G., and Hovius, N., eds., *Tectonic Faults, Agents of Change on a Dynamic Earth: Report of the 95th Dahlem Workshop on the Dynamics of Fault Zones*: Cambridge, Massachusetts, MIT Press, p. 357–401.
- Rosenberg, C.L., and Handy, M.R., 2005, Experimental deformation of partially melted granite revisited: Implications for the continental crust: *Journal of Metamorphic Geology*, v. 23, p. 19–28, doi:10.1111/j.1525-1314.2005.00555.x.
- Rutter, E.H., Brodie, K.H., and Irving, D.H., 2006, Flow of synthetic, wet, partially molten “granite” under undrained conditions: An experimental study: *Journal of Geophysical Research. Solid Earth*, v. 111, p. B06407, doi:10.1029/2005jb004257.
- Rutter, E.H., Mecklenburgh, J., and Brodie, K.H., 2011, Rock mechanics constraints on mid-crustal low-viscosity flow beneath Tibet, in Prior, D.J., Rutter, E.H., and Tatham, D.J., eds., *Deformation Mechanisms, Rheology and Tectonics: Microstructures, Mechanics, and Anisotropy*: Geological Society of London Special Publications, v. 360, p. 329–336, doi:10.1144/SP360.19.
- Scailliet, B., France-Lanord, C., and Le Fort, P., 1990, Badrinath-Gangotri plutons (Garhwal, India): Petrological and geochemical evidence for fractionation processes in a high Himalayan leucogranite: *Journal of Volcanology and Geothermal Research*, v. 44, p. 163–188, doi:10.1016/0377-0273(90)90017-A.
- Searle, M., 2013, Crustal melting, ductile flow, and deformation in mountain belts: Cause and effect relationships: *Lithosphere*, v. 5, p. 547–554, doi:10.1130/REFL006.1.
- Searle, M.P., 1986, Structural evolution and sequence of thrusting in the High Himalayan, Tibetan Tethys and Indus suture zones of Zaskar and Ladakh, western Himalaya: *Journal of Structural Geology*, v. 8, p. 923–936, doi:10.1016/0191-8141(86)90037-4.
- Searle, M.P., 2010, Low-angle normal faults in the compressional Himalayan orogen: Evidence from the Annapurna-Dhaulagiri Himalaya, Nepal: *Geosphere*, v. 6, p. 296–315, doi:10.1130/GES00549.1.
- Searle, M.P., 2015, Mountain building, tectonic evolution, rheology and crustal flow in the Himalaya, Karakorum and Tibet, in Schubert, G., ed., *Treatise on Geophysics*, Second Edition, Volume 6: Oxford, UK, Elsevier, p. 469–511, doi:10.1016/B978-0-444-53802-4.00121-4.
- Searle, M.P., and Godin, L., 2003, The South Tibetan Detachment and the Manaslu Leucogranite: A structural reinterpretation and restoration of the Annapurna-Manaslu Himalaya, Nepal: *The Journal of Geology*, v. 111, p. 505–523, doi:10.1086/376763.
- Searle, M.P., and Szulc, A.G., 2005, Channel flow and ductile extrusion of the high Himalayan slab—The Kangchenjunga-Darjeeling profile, Sikkim Himalaya: *Journal of Asian Earth Sciences*, v. 25, p. 173–185, doi:10.1016/j.jseae.2004.03.004.
- Searle, M.P., Simpson, R.L., Law, R.D., Parrish, R.R., and Waters, D.J., 2003, The structural geometry, metamorphic and magmatic evolution of the Everest massif, High Himalaya of Nepal-South Tibet: *Journal of the Geological Society*, v. 160, p. 345–366, doi:10.1144/0016-764902-126.
- Searle, M.P., Law, R.D., and Jessup, M.J., 2006, Crustal structure, restoration, and evolution of the Greater Himalaya in Nepal-South Tibet: Implications for channel flow and ductile extrusion of the middle crust, in Law, R.D., Searle, M.P., and Godin, L., eds., *Channel Flow, Ductile Extrusion and Exhumation in Continental Collision Zones*: Geological Society of London Special Publications, v. 268, p. 355–378, doi:10.1144/GSL.SP2006.268.01.17.
- Searle, M.P., Law, R.D., Godin, L., Larson, K.P., Streule, M.J., Cottle, J.M., and Jessup, M.J., 2008, Defining the Himalayan Main Central Thrust in Nepal: *Journal of the Geological Society*, v. 165, p. 523–534, doi:10.1144/0016-76492007-081.

- Searle, M.P., Cottle, J.M., Streule, M.J., and Waters, D.J., 2010, Crustal melt granites and migmatites along the Himalaya: melt source, segregation, transport and granite emplacement mechanisms: Sixth Hutton Symposium on the Origin of Granites and Related Rocks: Proceedings of a Symposium: Transactions of the Royal Society of Edinburgh, v. 100, p. 219–233, doi:10.1017/S175569100901617X.
- Searle, M.P., Elliott, J.R., Phillips, R.J., and Chung, S.L., 2011, Crustal-lithospheric structure and continental extrusion of Tibet: *Journal of the Geological Society*, v. 168, p. 633–672, doi:10.1144/0016-76492010-139.
- Streule, M.J., Searle, M.P., Waters, D.J., and Horstwood, M.S.A., 2010, Metamorphism, melting, and channel flow in the Greater Himalayan Sequence and Makalu leucogranite: Constraints from thermobarometry, metamorphic modeling, and U-Pb geochronology: *Tectonics*, v. 29, p. TC5011, doi:10.1029/2009TC002533.
- Turcotte, D.L., and Schubert, G., 2002, *Geodynamics*: Cambridge, UK, Cambridge University Press, doi:10.1017/CBO9780511807442.
- Unsworth, M.J., Jones, A.G., Wei, W., Marquis, G., Gokarn, S.G., Spratt, J.E., Bedrosian, P., Booker, J., Chen L.S., Clarke, G., Li, S.H., Lin, C.H., Ming, D., Sheng, J., Solon, K., Tan, H.D., Ledo, J., and Roberts, B., for The INDEPTH-MT team, 2005, Crustal rheology of the Himalaya and Southern Tibet inferred from magnetotelluric data: *Nature*, v. 438, p. 78–81, doi:10.1038/nature04154.
- Upreti, B.N., 1999, An overview of the stratigraphy and tectonics of the Nepal Himalaya: *Journal of Asian Earth Sciences*, v. 17, p. 577–606, doi:10.1016/S1367-9120(99)00047-4.
- Vannay, J.C., and Grasemann, B., 2001, Himalayan inverted metamorphism and syn-convergence extension as a consequence of a general shear extrusion: *Geological Magazine*, v. 138, p. 253–276, doi:10.1017/S0016756801005313.
- Vannay, J.C., and Hodges, K.V., 1996, Tectonometamorphic evolution of the Himalayan metamorphic core between the Annapurna and Dhaulagiri, central Nepal: *Journal of Metamorphic Geology*, v. 14, p. 635–656, doi:10.1046/j.1525-1314.1996.00426.x.
- Visonà, D., and Lombardo, B., 2002, Two-mica and tourmaline leucogranites from the Everest-Makalu region (Nepal-Tibet): Himalayan leucogranite genesis by isobaric heating?: *Lithos*, v. 62, p. 125–150, doi:10.1016/S0024-4937(02)00112-3.
- Walker, J.D., Martin, M.W., Bowring, S.A., Searle, M.P., Waters, D.J., and Hodges, K.V., 1999, Metamorphism, melting, and extension: Age constraints from the High Himalayan Slab of southeast Zaskar and northwest Lahaul: *The Journal of Geology*, v. 107, p. 473–495, doi:10.1086/314360.
- Webb, A.A.G., Yin, A., Harrison, T.M., Célérier, J., Gehrels, G.E., Manning, C.E., and Grove, M., 2011, Cenozoic tectonic history of the Himachal Himalaya (northwestern India) and its constraints on the formation mechanism of the Himalayan orogen: *Geosphere*, v. 7, p. 1013–1061, doi:10.1130/GES00627.1.
- White, R.W., Powell, R., and Holland, T.J.B., 2001, Calculation of partial melting equilibria in the system $\text{Na}_2\text{O}-\text{CaO}-\text{K}_2\text{O}-\text{FeO}-\text{MgO}-\text{Al}_2\text{O}_3-\text{SiO}_2-\text{H}_2\text{O}$ (NCKFMASH): *Journal of Metamorphic Geology*, v. 19, p. 139–153, doi:10.1046/j.0263-4929.2000.00303.x.
- Whitney, D.L., Teyssier, C., and Fayon, A.K., 2004, Isothermal decompression, partial melting and exhumation of deep continental crust, *in* Grocott, J., McCaffrey, K.J.W., Taylor, G., and Tikoff, B., eds., *Vertical Coupling and Decoupling in the Lithosphere*: Geological Society of London Special Publications, v. 227, p. 313–326, doi:10.1144/GSL.SP.2004.227.01.16.
- Williams, P.F., Jiang, D., and Lin, S., 2006, Interpretation of deformation fabrics of infrastructure zone rocks in the context of channel flow and other tectonic models, *in* Law, R.D., Searle, M.P., and Godin, L., eds., *Channel Flow, Ductile Extrusion and Exhumation in Continental Collision Zones*: Geological Society of London Special Publications, v. 268, p. 221–235, doi:10.1144/gsl.sp.2006.268.01.10.
- Yin, A., 2006, Cenozoic tectonic evolution of the Himalayan orogen as constrained by along-strike variation of structural geometry, exhumation history, and foreland sedimentation: *Earth-Science Reviews*, v. 79, p. 163–164, doi:10.1016/j.earscirev.2006.08.005.